




Article

Combustion-Synthesized Porous CuO-CeO₂-SiO₂ Composites as Solid Catalysts for the Alkenylation of C(sp³)-H Bonds Adjacent to a Heteroatom via Cross-Dehydrogenative Coupling

Ha V. Le ^{1,2,*}, Vy B. Nguyen ^{1,2}, Hai H. Pham ^{1,2}, Khoa D. Nguyen ^{1,2}, Phuoc H. Ho ^{3,†} , Philippe Trens ³  and Francesco Di Renzo ^{3,*} 

¹ Faculty of Chemical Engineering, Ho Chi Minh University of Technology (HCMUT), 268 Ly Thuong Kiet Street, District 10, Ho Chi Minh City 740010, Vietnam; vy.nguyenbich1012@hcmut.edu.vn (V.B.N.); phhai@hcmut.edu.vn (H.H.P.); khoand1989@hcmut.edu.vn (K.D.N.)

² Department of Organic Chemical Engineering, Vietnam National University Ho Chi Minh City, Linh Trung Ward, Thu Duc District, Ho Chi Minh City 740010, Vietnam

³ ICGM, University Montpellier-CNRS-ENSCM, Centre Balard, 34090 Montpellier, France; phuoc@chalmers.se (P.H.H.); philippe.trens@enscm.fr (P.T.)

* Correspondence: lvha@hcmut.edu.vn (H.V.L.); francesco.di-renzo@umontpellier.fr (F.D.R.)

† Present address: Chemical Engineering, Competence Centre for Catalysis, Chalmers University of Technology, SE-412 96 Gothenburg, Sweden.



Citation: Le, H.V.; Nguyen, V.B.; Pham, H.H.; Nguyen, K.D.; Ho, P.H.; Trens, P.; Di Renzo, F. Combustion-Synthesized Porous CuO-CeO₂-SiO₂ Composites as Solid Catalysts for the Alkenylation of C(sp³)-H Bonds Adjacent to a Heteroatom via Cross-Dehydrogenative Coupling. *Catalysts* **2021**, *11*, 1252. <https://doi.org/10.3390/catal11101252>

Academic Editors: Hironao Sajiki, Yoshinari Sawama and Igor M. Opsenica

Received: 7 October 2021

Accepted: 14 October 2021

Published: 18 October 2021

Publisher's Note: MDPI stays neutral with regard to jurisdictional claims in published maps and institutional affiliations.



Copyright: © 2021 by the authors. Licensee MDPI, Basel, Switzerland. This article is an open access article distributed under the terms and conditions of the Creative Commons Attribution (CC BY) license (<https://creativecommons.org/licenses/by/4.0/>).

Abstract: A series of mixed oxides of CuO, CeO₂, and SiO₂ were prepared by gel combustion and employed for the first time as efficient solid catalysts in a solvent-less liquid-phase cross-dehydrogenative coupling. The facile one-pot catalyst synthesis resulted in highly porous materials presenting large specific surface areas and strong metal-support interactions. The interaction with highly dispersed CeO₂ enhanced the redox properties of the CuO species. The CuO-CeO₂-SiO₂ composites exhibited excellent catalytic performance for the selective coupling between 1,1-diphenylethylene and tetrahydrofuran with a yield up to 85% of 2-(2,2-diphenylvinyl)-tetrahydrofuran in the presence of di-*tert*-butyl peroxide (DTPB) and KI. Albeit both CuO and CeO₂ species are proved to be responsible for the catalytic conversion, a great synergistic improvement in the catalytic activity was obtained by extended contact between the oxide phases by high porosity in comparison with the reactions using individual Cu or Ce catalysts. The activity of the composite catalyst was shown to be highly stable after five successive reaction cycles. Furthermore, the study scope was extended to the synthesis of different derivatives via composite-catalyzed coupling of C(sp²)-H with C(sp³)-H adjacent to a heteroatom. The good yields recorded proved the general validity of this composite for the cross-dehydrogenative coupling reaction rarely performed on solid catalysts.

Keywords: mixed oxides; synergistic effect; cross-dehydrogenative coupling; alkenylation; solid catalyst

1. Introduction

In recent years, cross-dehydrogenative coupling (CDC) to directly build a C-C bond from two simple C-H bonds has emerged as an attractive goal in organic synthesis [1,2]. Offering great benefits including improving atom economy, step efficiency, and reducing cost and waste, the CDC reaction is a more efficient synthetic protocol to access product molecules compared to traditional cross-couplings, which often require the use of pre-functionalized halides and organometallic reagents [1,3–5]. In particular, α -C(sp³)-H of ethers and amines can be selectively coupled with C(sp³)-H or C(sp²)-H, leading to more complex structural motifs which have been usually found in natural products, pharmaceuticals, agrochemicals, biologically active molecules, and functional materials [6–8]. The CDC for the α -functionalization of ethers and amines is still a grand challenge because of the inert and ubiquitous nature of the C(sp³)-H bond. Many efforts to expand this convenient method have been reported in the past decade, in which first-row transition

metals, namely copper, iron, cobalt, are the most used catalysts [6,9–12]. Liu and co-workers investigated the α -functionalization of ethers with olefins in the presence of CuI catalyst to obtain α -alkenylated ethers [13]. Furthermore, the FeCl₃- or CoCl₂-catalyzed CDC between α -C(sp³)-H of ethers and C(sp²)-H of coumarin derivatives has been also reported [5,14]. These works were focused on CDC via homogeneous catalysis, whose production, purification, and environmental impacts raise significant concerns. From the perspective of green chemistry, it is, therefore, crucial to developing solid catalysts-mediated routes which allow easy catalyst separation and recycling and reduce product contamination. Khang and co-workers have recently synthesized α -functionalized ethers via CDC in the presence of a perovskite-based catalyst, in which doping LaCoO₃ with Sr was required to obtain significantly improved catalytic activity [15]. In general, the use of recyclable heterogeneous catalytic systems for the α -alkenylation of C(sp³)-H has been rarely reported in the literature.

CuO-CeO₂ catalysts have attracted more and more attention due to their low cost, high activity, and wide application in gas-phase catalysis [16–20]. Several mechanistic studies on the catalytic CuO-CeO₂ systems have suggested that high oxygen storage capacity and release capability in the lattice of the fluorite-like cubic structure of ceria and its strong interaction with CuO lead to the formation of a redox pair, namely Ce⁴⁺/Ce³⁺ and Cu²⁺/Cu⁺, with enhanced redox properties, thereby promoting the rate of catalyzed reactions at the metal–oxide interface [16,17,19,21–30]. It was also found that the preparation conditions had a significant influence on the particle size and dispersion as well as on the interaction of oxide species in the composites, which in turn strongly affect the catalytic performance [17,27,28,31]. To date, various methods to synthesize CuO-CeO₂ composites have been reported, including solution combustion, thermal decomposition, sol-gel, hydrothermal treatment, chemical vapor deposition co-precipitation, impregnation, mechanical milling [27,29,31–33]. Among them, the solution combustion synthesis, which is based on a cascade of fast and self-sustained redox reactions in a homogeneous solution of reagents containing metal cations, finally forming homogeneous oxide particles, has been considered as an excellent protocol in terms of simplicity of equipment and procedure, energy and time efficiency, product quality, and possibility of obtaining a desired composition [34–41]. However, combustion-synthesized CuO-CeO₂ mixed oxides usually had a poor porosity with low surface areas of 15–80 m² g^{−1} because of the uncontrollable sintering of particles at high temperatures [16,23,31,42–48]. In several studies, silica precursors were therefore added to the combustion solution to improve the composite porosity and the dispersion of active sites [49–53].

Due to the above-described unique characteristics, the catalytic activity of Cu- and Ce-containing mixed oxides was greatly improved compared to the corresponding individual counterparts and was even comparable to that of supported noble metal catalysts in numerous gas-phase reactions, such as oxidation of CO and hydrocarbons, water–gas shift, reduction of NO, reduction of SO₂ by CO, decomposition of ammonia, combustion of volatile organic compounds, epoxidation of propylene, wet oxidation of phenol, epoxidation of propylene [18,20,24,27,31,42,54,55]. Nevertheless, the well-known CuO-CeO₂ composite was rarely applied for liquid-phase organic transformations, despite the synergistic effect of the metal species on the catalysis has been proved to be indeed promising. Herein, we synthesized a series of porous composites containing CuO, CeO₂, and SiO₂ by the combustion method and investigated their catalytic activity in the dehydrogenative alkylation of C(sp³)-H adjacent to heteroatoms. The mixed oxides catalysts exhibited superior yields compared to single oxides and salts of copper and cerium or even to their physical mixture. To our best knowledge, combustion preparation and application of porous CuO-CeO₂-SiO₂ mixed oxides for the cross-dehydrogenative coupling between C(sp³)-H and C(sp²)-H have not yet been reported in the literature.

2. Results and Discussion

2.1. Catalyst Characterization

The composites consisting of CuO, CeO₂, and SiO₂ with varied compositions were simply prepared via gel combustion. After dissolving precursors including metal nitrate and TEOS into ethanol and slow removal of most of the ethanol from the mixture, a gel phase containing precursors and remained ethanol was formed. Combustion of such a gel mixture at 500 °C in air caused rapid condensation of the precursors in mixed oxides of CuO, CeO₂, and SiO₂ (Table 1). The samples were named as Cu₁Ce_xSi, where x was the analyzed Ce/Cu atomic ratio. XRD patterns of the composite samples showed different phases of mixed oxides, depending on the sample composition (Figure 1). A broad peak at approximately $2\theta = 22.5^\circ$ present in the patterns of all samples was assigned to amorphous silica [56]. The diffractogram of CuSi showed two sharp peaks at $2\theta = 36^\circ$ and 39° corresponding to (022) and (111) planes of the monoclinic CuO phase, indicating the formation of CuO in the composites [56,57]. As expected, new peaks at $2\theta = 28.5^\circ, 33^\circ, 47.4^\circ, 56.3^\circ$ were observed in the patterns of the Ce-containing composites. These diffraction peaks are indexed as (111), (200), (220), and (311) planes, respectively, corresponding to the cubic fluorite structure of the CeO₂ phase [58]. Using Scherrer's equation, the average crystallite size of CuO was 23 ± 1 nm and the crystallite size of CeO₂ was 5 ± 0.2 nm.

Table 1. Detailed amount of precursors for the preparation of CuO-CeO₂-SiO₂ composites.

Amount of Precursors (mmol)			Composite Sample ^[a]
Cu(NO ₃) ₂ ·3H ₂ O	Ce(NO ₃) ₃ ·6H ₂ O	TEOS	
6.3	0	83.2	CuSi
6.3	1.0	83.2	Cu ₁ Ce _{0.15} Si
6.3	3.0	83.2	Cu ₁ Ce _{0.45} Si
6.3	4.4	83.2	Cu ₁ Ce _{0.7} Si
6.3	6.0	83.2	Cu ₁ Ce _{0.91} Si

^[a] Name based on the actual atomic ratio of Cu:Ce in the as-prepared materials via ICP-OES analysis.

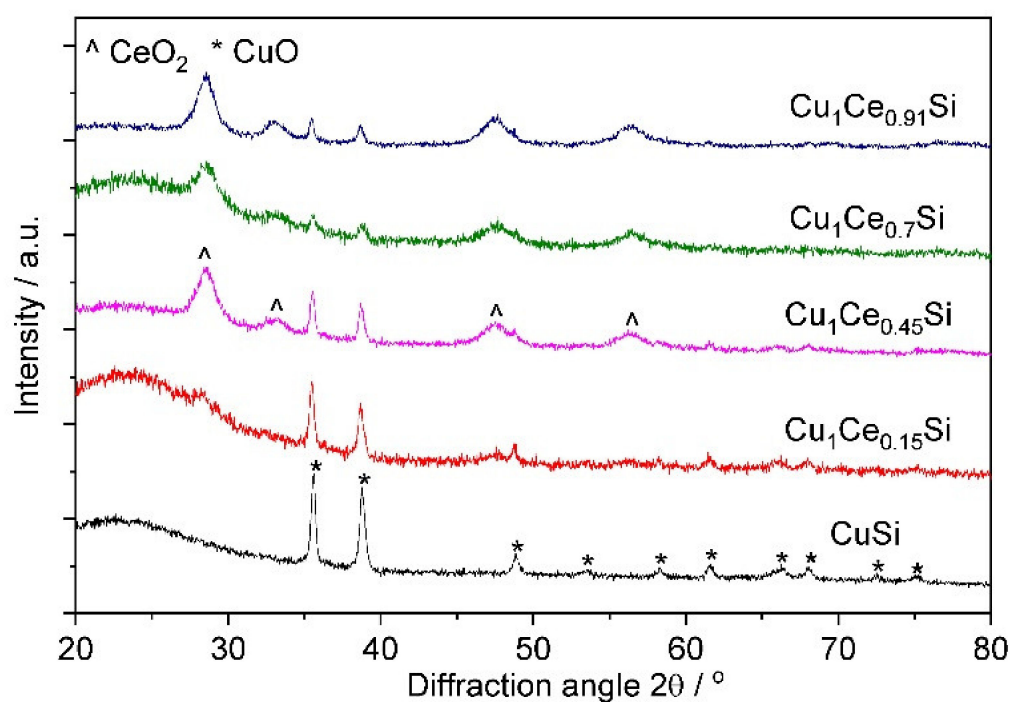


Figure 1. PXRD patterns of the as-prepared composite materials.

The redox properties of the composites were investigated via H₂-TPR analyses (Figure 2). As it can be expected, a broad peak was recorded below 300 °C and attributed to the reduction of CuO in the samples, consistently with previous studies. Notably, the onset of the reduction peak of CuO in the Ce-containing samples shifted to lower temperatures with the increase in the Ce loading, as reported in the literature for several CuO-CeO₂ composites [47,59–62]. In the case of CuO deposited on several silica supports, Le and co-workers have found that small CuO clusters at more accessible positions in the silica-based materials (i.e., outer surface, large pores) were reduced more easily than ones at small pores and bulk CuO [57,63]. In the case of transition metals supported on CeO₂, it was suggested that active sites for oxidation reactions were located at the contact between the dispersed transition metal and CeO₂ [64,65]. In our case, it can be explained that the incorporation of small nanocrystals of CeO₂ largely increased the extent of the interface between CuO species and CeO₂, an effect that enhanced the reducibility of CuO [66,67]. Indeed, it was suggested that CeO₂ on the surface of silica promoted the strong interaction of CuO species with ceria, leading to H₂ consumption at a low-temperature range of 150–200 °C, as observed in earlier studies on CuO and CeO₂ mixed oxides [24,25,47,59,68–70].

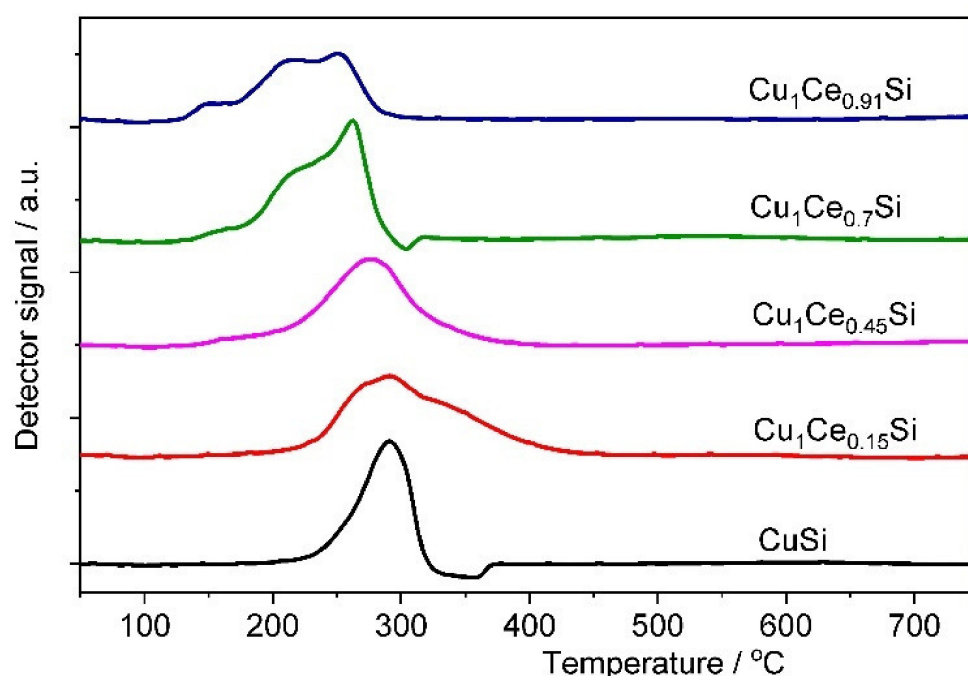


Figure 2. H₂-TPR profiles of the as-prepared composites.

Upon quantification of H₂ consumptions for the TPR experiments of the composites, all Cu/H₂ molar ratios were found to be in the range 1.03–1.09, close to the stoichiometric ratio for the reduction of Cu²⁺ to Cu⁰, verifying that most H₂ consumption indeed corresponded to the reduction of Cu(II) species (Table S1). Generally, a pure CeO₂ phase could be incompletely reduced in two steps, namely, at ~520 °C for the reduction of surface ceria and ~750–900 °C for the reduction of bulk ceria [60,71]. The bulk oxygen is strongly bonded with Ce in the crystalline structure of CeO₂; therefore, it reacts with H₂ at a higher temperature compared to the surface oxygen of CeO₂. However, in this work, no reduction peaks were observed in such a temperature range for the Ce-containing samples probably because the H₂ consumption for the reduction of CeO₂ with low contents (i.e., 2–12 wt.%) was negligible. Indeed, the typical H₂ consumption on the low-temperature TPR peak of high-surface area CeO₂ is about 0.7 mmol H₂/g CeO₂, to be compared with 25 mmol H₂/g CuO for the CuO reduction peaks [71]. A missed observation of the CeO₂ reduction peak at low temperature has been also reported for TPR profiles of CeO₂-containing composites in earlier studies [25,33,59,70,72].

The gel combustion route is based on exothermic redox reactions between nitrates as oxidizers and organic substances as reducers in a homogeneous solution to directly produce nano-structured oxides [36,38]. Such a process emits explosively a large number of gaseous byproducts in a short time, not only inhibiting the particle growth but also making the oxides highly porous and finely dispersed [16,40]. These expected features could be confirmed via SEM and isothermal nitrogen sorption measurements [35,38]. The SEM images showed that the incorporation of Ce substantially influences the morphology and particle size of the composites (Figure 3). Large particles with irregular shapes were observed on the CuSi sample (Figure 3a) while more homogeneous and smaller particles were generated when Ce was added to the composite. Spherical nanoparticles smaller than 100 nm were indeed observed for the composite containing more than 3.26 wt.% of Ce (Figure 3c–e). Additionally, SEM/EDX elemental mapping analysis (Figure S1) indicated a homogeneous dispersion of Cu, Ce, and Si species throughout the composite.

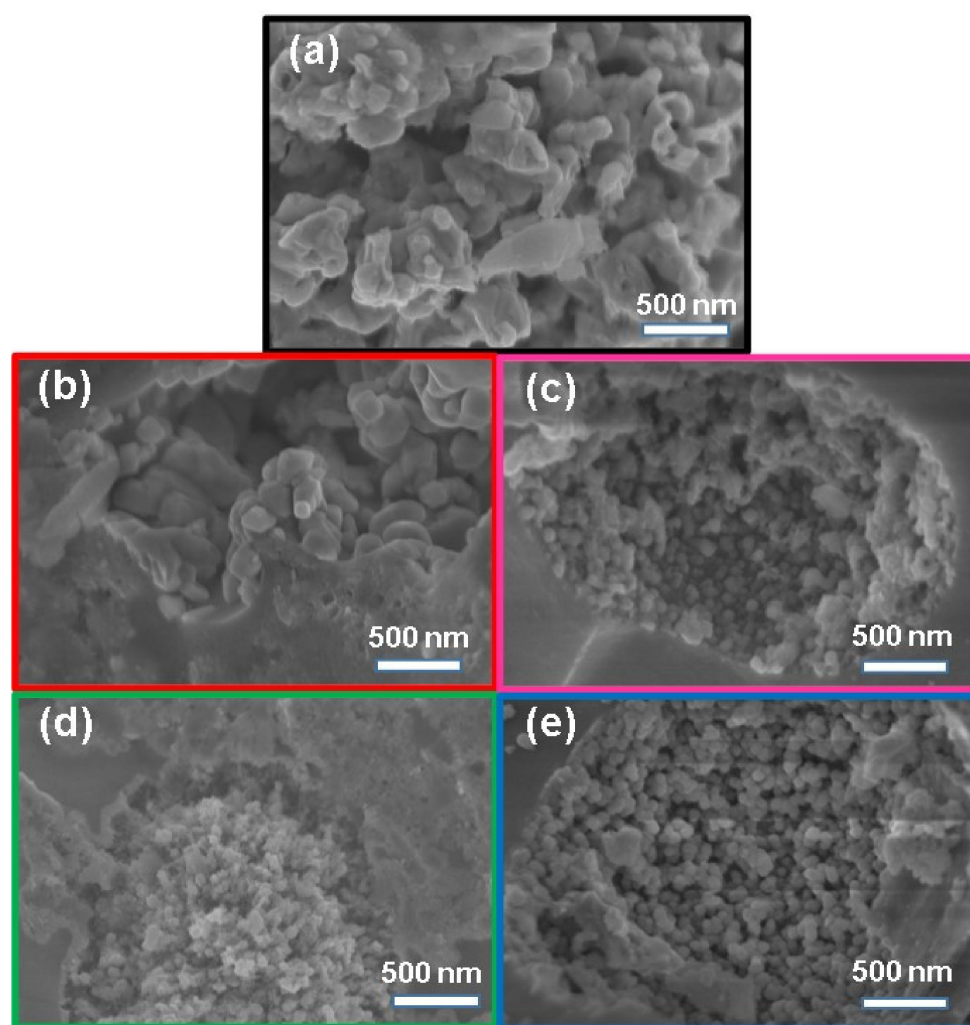


Figure 3. SEM images of (a) CuSi, (b) $\text{Cu}_1\text{Ce}_{0.15}\text{Si}$, (c) $\text{Cu}_1\text{Ce}_{0.45}\text{Si}$, (d) $\text{Cu}_1\text{Ce}_{0.7}\text{Si}$, and (e) $\text{Cu}_1\text{Ce}_{0.91}\text{Si}$.

The nitrogen physisorption isotherms of the samples at 77 K presented type I isotherms, which are typical for microporous materials with a small extent of the outer surface (Figure 4) [73]. Microporous silica xerogels are easily prepared by condensation of silica precursors in acidic solutions, also in the presence of ethanol or other organic solvents [74–76]. The pore size distribution results calculated from the N_2 adsorption data showed that the pores formed in the composite were mainly smaller than 2 nm in diameter (Figure S2). Indeed, only 5–10% of the total pore volumes were contributed by

mesopores present in the composites (Table 2). In fact, CuO-CeO₂ composites synthesized via the solution combustion method were usually found to possess low surface areas due to the high density of the oxides [16,23,31,42–46]. Therefore, in this combustion route, a large amount of silica precursors was used to improve the composite porosity. In several previous studies, combustion-synthesized materials were prepared in the presence of pre-shaped mesoporous silica and retained the mesoporosity of the silica support [47,48,51]. When soluble silica precursors were used in the synthesis, materials with homogeneous microporosity were obtained for transition metal/silica molar ratio up to 30%, whereas mixed micropore-mesopore distributions were obtained for higher transition metal contents [53]. The BET surface area of materials from CuSi to Cu₁Ce_{0.7}Si was $370 \pm 10 \text{ m}^2 \text{ g}^{-1}$, in good agreement with literature reports for combustion-synthesized composites containing silica [49,50,53]. At higher cerium content, the surface area decreased to $260 \text{ m}^2 \text{ g}^{-1}$ for Cu₁Ce_{0.91}Si, which also presented the largest mesopore volume fraction (11 %), suggesting the formation of more tightly packed crystallite aggregates. These porosity results demonstrated the great efficiency of this method for the preparation of a highly porous composite material containing CuO, CeO₂, and SiO₂.

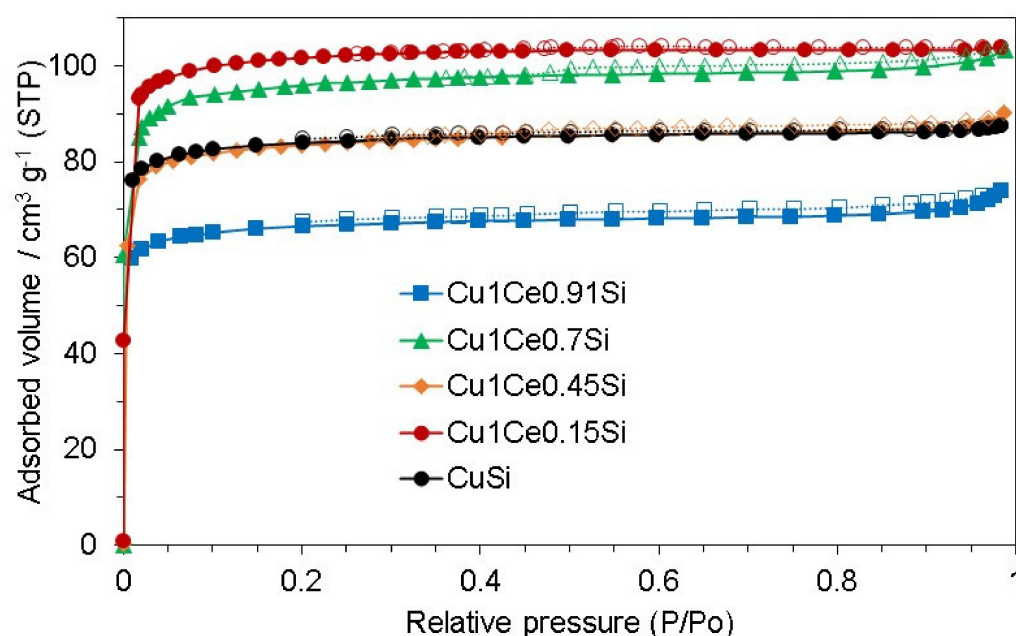


Figure 4. N₂-physisorption isotherms of the combustion-synthesized composites.

Table 2. Composition and textural properties of synthesized composite materials.

Entry	Composite Sample	Obtained Molar Composition of Cu:Ce [a]	Cu Content [a] (wt.%)	Ce Content [a] (wt.%)	SA [b] (m ² g ^{−1})	V _{micro} [c] (cm ³ g ^{−1})	V _{total} [d] (cm ³ g ^{−1})
1	CuSi	-	7.44	0	340	0.129	0.136
2	Cu ₁ Ce _{0.15} Si	1Cu:0.15Ce	7.17	2.37	411	0.156	0.160
3	Cu ₁ Ce _{0.45} Si	1Cu:0.45Ce	6.69	6.64	337	0.127	0.140
4	Cu ₁ Ce _{0.7} Si	1Cu:0.7Ce	6.48	10.00	389	0.145	0.155
5	Cu ₁ Ce _{0.91} Si	1Cu:0.91Ce	6.22	12.35	262	0.102	0.115

[a] Determined by ICP-OES analysis. [b] SA = surface area calculated by the BET method. [c] V_{micro} = micropore volume calculated by the αS method. [d] V_{total} = total pore volume calculated at p/p₀ = 0.99.

2.2. Catalytic Study

2.2.1. Optimization of Reaction Conditions

The combustion-synthesized CuO-CeO-SiO₂ composites were applied as solid catalysts for the cross-dehydrogenative coupling of 1,1-diphenylethylene with tetrahydrofuran to produce 2-(2,2-diphenylvinyl)-tetrahydrofuran as the major product (Figure 5). Reaction conditions were intensively screened to improve the product yield. Initially, the influence of the reaction temperature on the direct alkenylation of the C(sp³)-H bond adjacent to the oxygen atom of tetrahydrofuran was explored (Figure 6). In particular, the coupling reaction was carried out at different temperatures in the range of ambient temperature to 140 °C for 20 h using 3.2 mol% of the Cu₁Ce_{0.7}Si catalyst in the presence of 4 equiv. of DTBP as an oxidant and 20 mol% of KI as an additive. In this synthetic route, no additional organic solvent was required as excess tetrahydrofuran was applied as both reactant and solvent for the reaction.

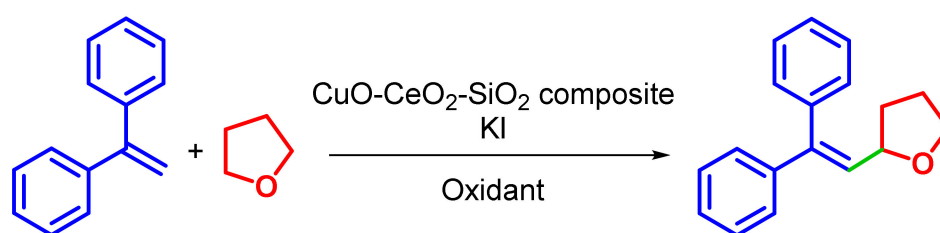


Figure 5. The cross-dehydrogenative coupling of 1,1-diphenylethylene with tetrahydrofuran catalyzed by the CuO-CeO₂-SiO₂ composite.

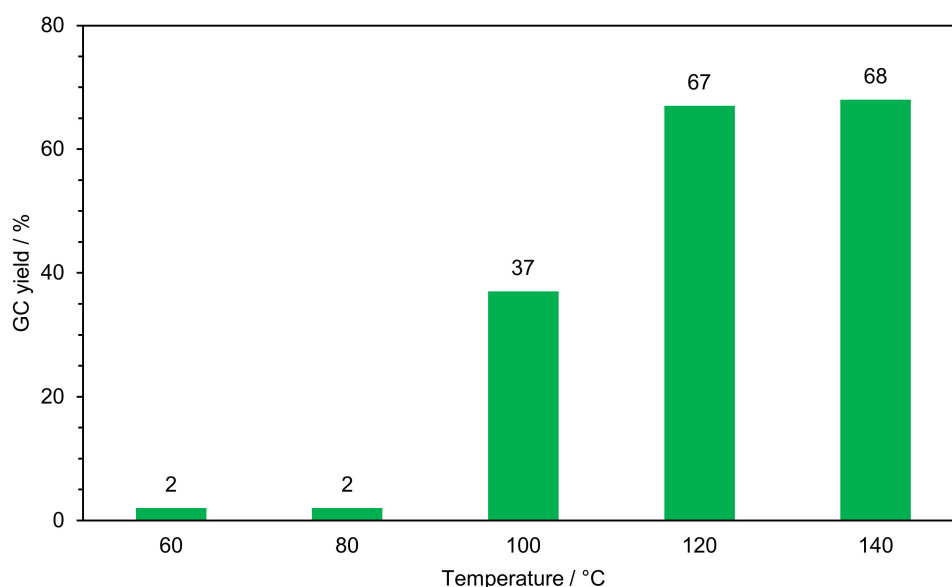


Figure 6. Effect of the reaction temperature on the product yield. Reaction conditions: 1,1-diphenylethylene (0.3 mmol); THF (1 mL); KI (20 mol%); DTBP (4 equiv.); Cu₁Ce_{0.7}Si catalyst (5.6 mg); under air for 20 h.

The results showed that the reaction proceeded negligibly below 80 °C, with only 2% of the desired product detected after 20 h. It should be noted that the peroxide bond of DTBP undergoes homolysis at temperatures above 100 °C, yielding a steady concentration of the initiating radical for the carbon–carbon bond-forming reactions [77–79]. Correspondingly, the reaction carried out at 100 and 120 °C gave significantly higher product yields of 37% and 67%, respectively. However, no further enhancement in the formation of the major product was observed when increasing the reaction temperature to 140 °C. Indeed, the dehydrogenative alkenylations of ethers catalyzed by molecular Cu salts were performed

at 120 °C in the earlier studies, implying that this temperature condition was not only appropriate for selective activation and coupling of C(sp²)-H and C(sp³)-H bonds but also controlled the unexpected oxidation of alkene substrates in the presence of the DTBP oxidant [13,15,80,81]. In the work on oxidative coupling, Trinh and co-workers also reported that the oxidation of 1,1-diphenylethylene to benzophenone by DTBP was significant at 140 °C [82].

Similar to other cross-dehydrogenative coupling reactions, no alkenylation of THF occurred in the absence of an oxidant. Therefore, various organic and inorganic oxidants were tested for the reaction (Figure 7). The results showed that this transformation strongly depended on the oxidant nature. The tested inorganic oxidants including K₂S₂O₈ and H₂O₂ were found to be unsuitable for the direct coupling of 1,1-diphenylethylene with THF with negligible yields lower than 3% recorded after 20 h. Similar results were also obtained for the cases of TBHP in either water or decane, *tert*-butyl peroxybenzoate, and TEMPO, while the reaction could proceed slowly in the presence of PhI(OAc)₂ as the oxidation, affording a poor yield of 10%. In the oxidant series, DTBP emerges as the best choice, producing 2-(2,2-diphenylvinyl)-tetrahydrofuran in the 67% yield.

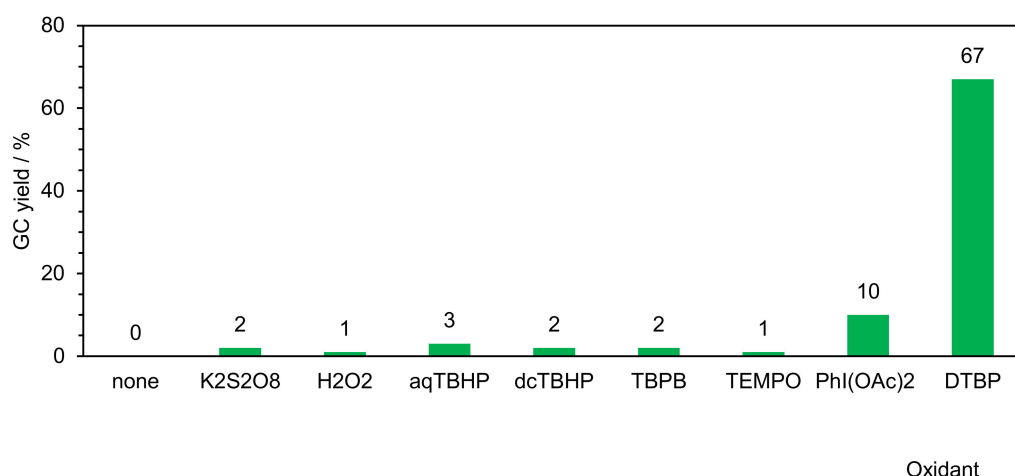


Figure 7. Effect of the oxidant on the product yield. Reaction conditions: 1,1-diphenylethylene (0.3 mmol); THF (1 mL); KI (20 mol%); oxidant (4 equiv.); Cu₁Ce_{0.7}Si catalyst (5.6 mg); 120 °C; under air for 20 h. DTBP: di-*tert*-butylperoxide; aqTBHP: *tert*-butyl hydroperoxide in water; dcTBHP: *tert*-butyl hydroperoxide in decane; TBPB: *tert*-butyl peroxybenzoate, TEMPO: (2,2,6,6-tetramethylpiperidin-1-yl)oxyl.

Furthermore, the impact of the oxidant amount was studied, displaying that increasing the DTBP amount from 1 to 4 equiv. gave increased yields (Figure 8). Using 5 equiv. of DTBP was found unnecessary for this transformation, with the same yield as the reaction with 4 equiv. of DTBP. Notably, the yield of 2-(2,2-diphenylvinyl)-tetrahydrofuran was dropped to 23% when 6 equiv. of DTBP were added to the reaction probably due to significantly accelerating the oxidation of 1,2-diphenylethylene. The product could be obtained in the absence of KI but with a slow rate, giving a low yield of 31% (Figure 9). As expected, adding KI to the reaction led to a significant improvement in the formation of the major product, confirming the promoting role of KI in this cross-dehydrogenative coupling of 1,1-diphenylethylene with THF, which significantly depends on its amount. A yield of 67% could be obtained with 20 mol% of KI, more than double of the KI-free case. However, further increasing the KI amount, i.e., from 20 to 25 mol%, was ineffective as the product yield slightly decreased from 67 to 64%.

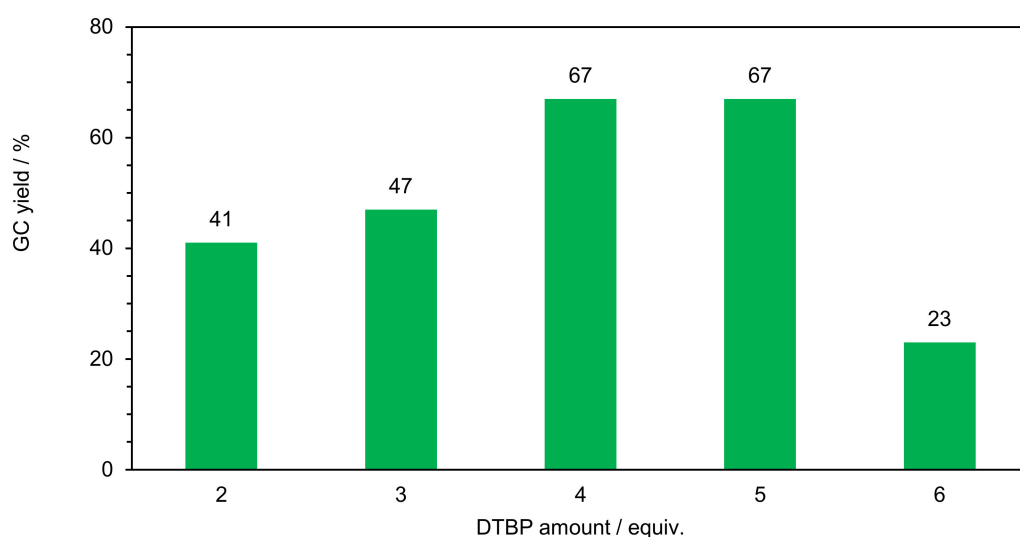


Figure 8. Effect of the amount of the DTBP oxidant on the product yield. Reaction conditions: 1,1-diphenylethylene (0.3 mmol); THF (1 mL); KI (20 mol%); $\text{Cu}_1\text{Ce}_{0.7}\text{Si}$ catalyst (5.6 mg); 120 °C; under air for 20 h.

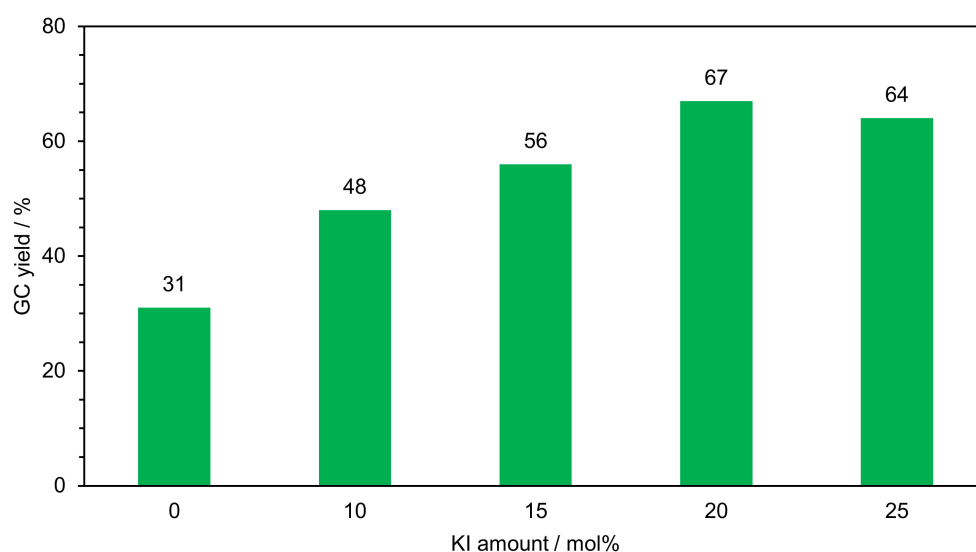


Figure 9. Effect of the amount of the KI additive on the product yield. Reaction conditions: 1,1-diphenylethylene (0.3 mmol); THF (1 mL); DTBP (4 equiv.); $\text{Cu}_1\text{Ce}_{0.7}\text{Si}$ catalyst (5.6 mg); 120 °C; under air for 20 h.

The effect of the $\text{Cu}_1\text{Ce}_{0.7}\text{Si}$ catalyst amount on the reaction of 1,1-diphenylethylene and tetrahydrofuran is shown in Figure 10. Given that both Cu and Ce species were active for the transformation, the catalyst amount was determined based on the total molar number of these catalytic sites. No major product was detected after 20 h without catalyst, verifying the essential role of the Cu- and Ce-containing composite for this coupling. Obviously, the reaction rate could be accelerated by increasing the catalyst amount. The desired product was obtained in yields of 38, 67, and 78% within 20 h in the presence of 2.8, 5.6, and 8.4 mg of $\text{Cu}_1\text{Ce}_{0.7}\text{Si}$, which are equal to 1.6, 3.2, and 4.8 mol%, respectively. Nevertheless, extending the catalyst amount to 11.2 mg (6.5 mol%) did not lead to any enhancement in the production of 2-(2,2-diphenylvinyl)-tetrahydrofuran under identical conditions. It should be emphasized that the $\text{Cu}_1\text{Ce}_{0.7}\text{Si}$ catalyst showed a high performance at significantly lower amounts compared to the case of similar couplings under homogeneous catalysis, in which transition metal salts were used in the range of

10–20 mol% [5,13,14,80,83]. Furthermore, the kinetic investigation of the reaction revealed that the cross-dehydrogenative coupling steadily increased with reaction time (Figure 11). The highest product yield was 85% at 25 h. The decrease of yield for a longer reaction time can be rationalized by the fact that the alkene bond present in the product has high reactivity toward competitive oxidative reactions.

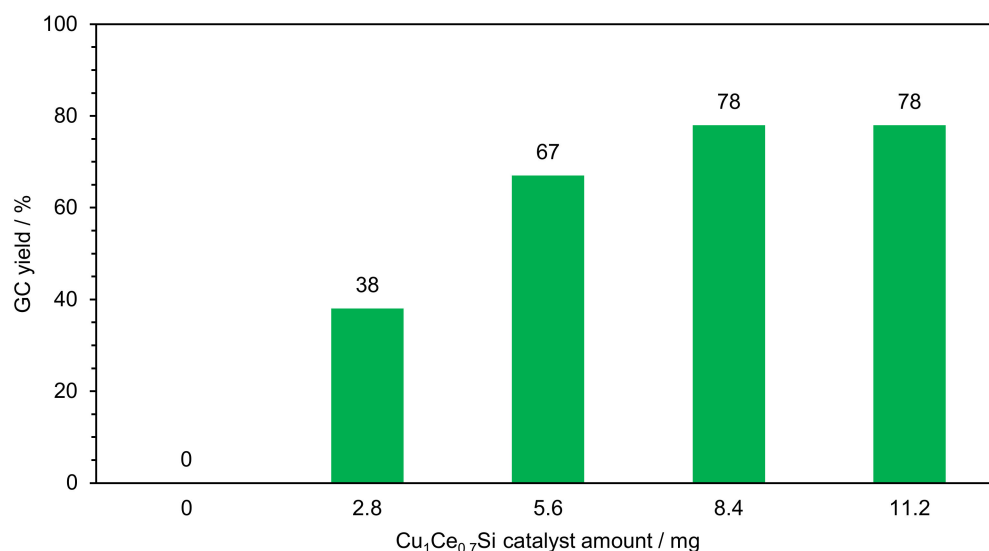


Figure 10. Effect of the amount of the Cu₁Ce_{0.7}Si catalyst on the product yield. Reaction conditions: 1,1-diphenylethylene (0.3 mmol); THF (1 mL); DTBP (4 equiv.); KI (20 mol%); 120 °C; under air for 20 h.

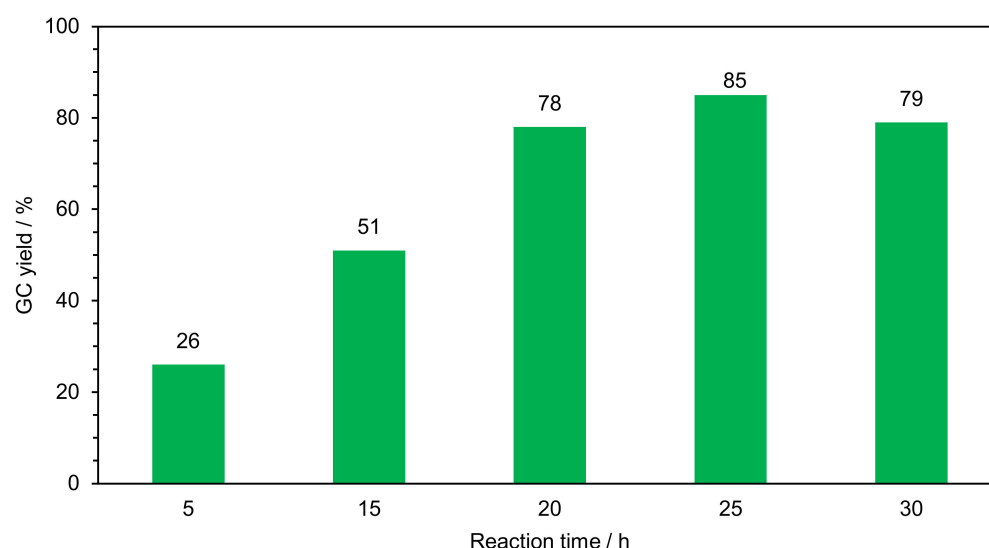


Figure 11. Effect of the reaction time on the product yield. Reaction conditions: 1,1-diphenylethylene (0.3 mmol); THF (1 mL); DTBP (4 equiv.); KI (20 mol%), Cu₁Ce_{0.7}Si catalyst (8.4 mg–4.8 mol%); 120 °C; under air.

2.2.2. Comparison of Catalysts

With these results in mind, the catalytic activity of CuO-CeO₂-SiO₂ catalysts with different compositions for the coupling of 1,1-diphenylethylene with THF was explored (Table 3, entries 1–5, and Figure 12). The reactions were conducted in 25 h using 4.8 mol% of the metal sites, 4 equiv. of DTBP, and 20 mol% of KI. Interestingly, although the amount of the total metal sites was kept constant for the experiments, the presence of Ce in the

composite resulted in higher yields of 2-(2,2-diphenylvinyl)-tetrahydrofuran (Entries 1–4) in comparison with the Ce-free case of CuSi (33% yield, Entry 5). The formation of 5 nm CeO₂ nanocrystals improved the contact with the CuO phase and the yield increased with the cerium content until, for the Cu₁Ce_{0.7}Si composite, a yield of 85% was recorded. For higher cerium content, a decrease of accessibility, due to the aggregation of nanoparticles witnessed by the decrease of surface area, accounted for a decrease of yield to 62% on the Cu₁Ce_{0.91}Si catalyst.

Table 3. Catalytic performance of Cu- and Ce-based catalysts in the cross-dehydrogenative coupling^a between THF and 1,1-diphenylethylene.

Entry	Catalyst(s)	Used Cu Amount (mol%)	Used Ce Amount (mol%)	Yield ^{[a],[b]} (%)
1	Cu ₁ Ce _{0.91} Si	2.5	2.3	62
2	Cu ₁ Ce _{0.7} Si	2.8	2.0	85
3	Cu ₁ Ce _{0.45} Si	3.3	1.5	51
4	Cu ₁ Ce _{0.15} Si	4.2	0.6	45
5	CuSi	4.8	-	33
6	CuSi + CeO ₂	2.8	2.0	64
7	Cu(OAc) ₂	4.8	-	21
8	Cu(OAc) ₂ + CeO ₂	2.8	2.0	43
9	CuO	4.8	-	20
10	CuO + CeO ₂	2.8	2.0	25
11	CeO ₂	-	4.8	30
12	CuI	4.8	-	74
13	CuI + CeO ₂	2.8	2.0	64

^[a] Reaction conditions: 1,1-diphenylethylene (0.3 mmol); THF (1 mL); DTBP (1.2 mmol); KI (20 mol%); (4.8 mol%); 120 °C; under air for 25 h. ^[b] GC yield.

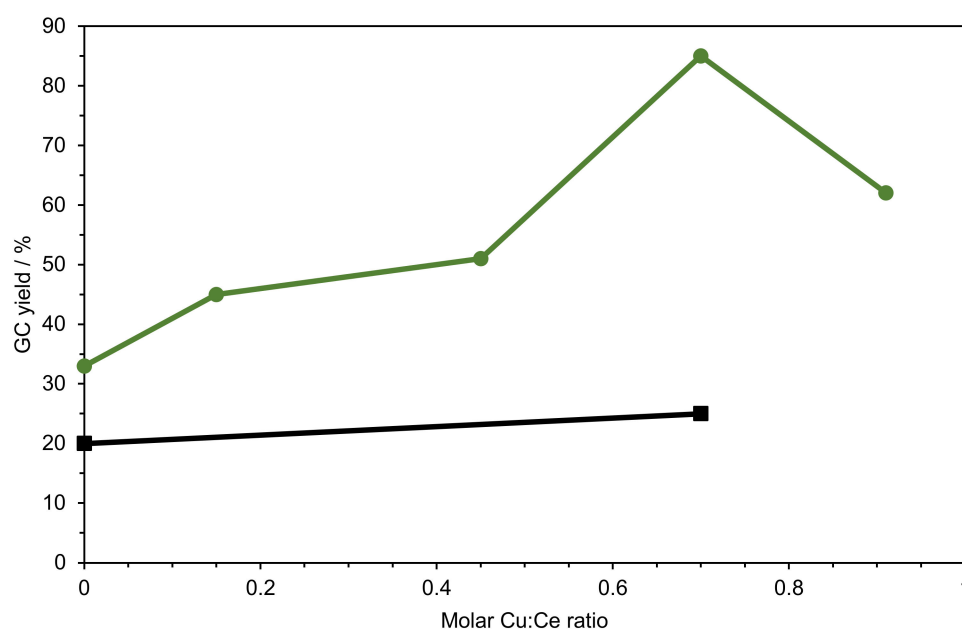


Figure 12. Yield of 2-(2,2-diphenylvinyl)-tetrahydrofuran vs. molar Ce:Cu ratio in CuO-CeO₂-SiO₂ composites from solution combustion (solid circle) and CuO-CeO₂ mechanical mixtures (solid square).

To gain more insights into possible active sites for this reaction, a series of Ce- and Cu-based catalytic systems were tested under identical conditions at the total metal amount of 4.8 mol%. The major product could be achieved in the presence of either Ce or Cu-containing materials, confirming that both Ce and Cu species are responsible for the

selective cross-dehydrogenative coupling between 1,1-diphenylethylene and THF (Table 3). According to the previous studies, a plausible redox cycle for the direct alkenylation of THF with 1,1-diphenylethylene catalyzed by the $\text{Cu}_1\text{Ce}_{0.7}\text{Si}$ catalyst was proposed (Figure 13) [12,13,15,78,83,84]. First, decomposition of DTBP into *tert*-butoxy radicals is accelerated at high temperatures in the presence of transition metal species [12,77,79,84]. The formation of the radicals from DTBP can occur on the active sites in the micropores. These highly reactive radicals would activate the $\text{C}_{\text{sp}^3}\text{-H}$ bond adjacent to the oxygen atom of THF via abstracting this hydrogen atom to form a cyclic ether radical which can subsequently diffuse from the micropores to the outer surface for the reaction with the bulky 1,1-diphenylethylene molecule, yielding a benzylic-based radical [78,85]. The conversion of the radical into the desired product takes place via the oxidation by the complex $[\text{M}^{\text{n}+1}\text{-O}^t\text{Bu}]$ to release $^t\text{BuOH}$ and regenerate $\text{M}^{\text{n}+}$ for the catalytic cycle [12,82]. The fact that adding TEMPO as a radical scavenger to the reaction led to no formation of the coupling product could strengthen this radical mechanism. The additional use of KI as a promoting agent was commonly reported in the Cu(II)-mediated coupling reaction [83,86,87]. It was believed that KI can facilitate the formation of *tert*-butoxy radicals from the redox reaction with DTBP and I_2 subsequently formed can promote the oxidation of $\text{M}^{\text{n}+}$ species [83,88].

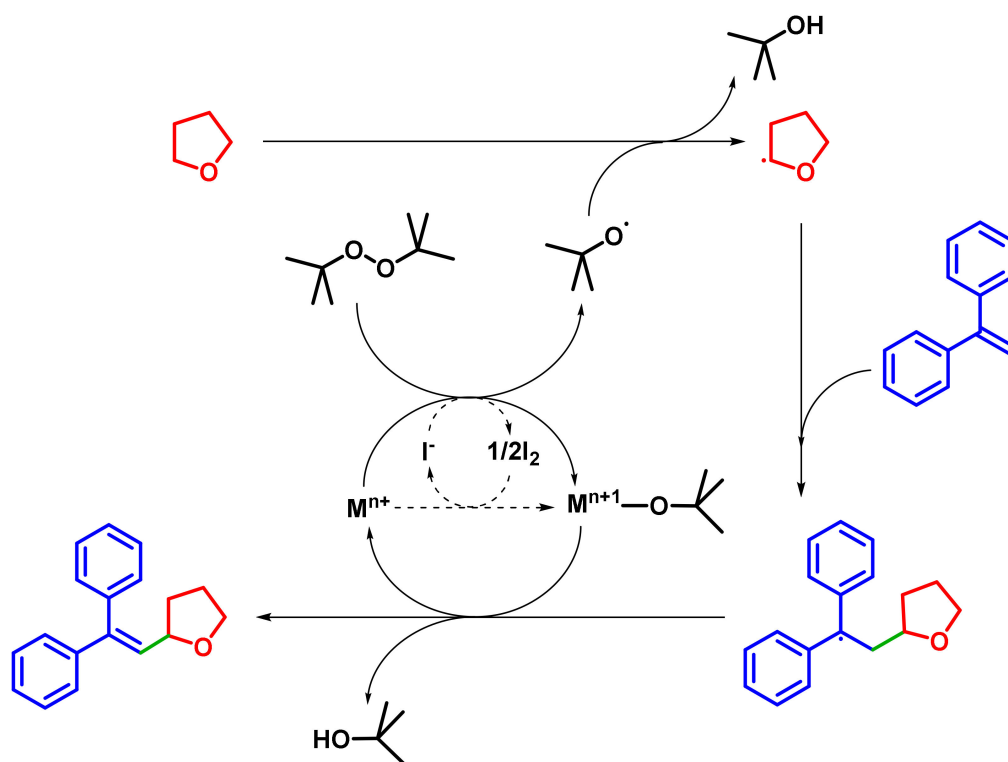


Figure 13. Proposed redox cycle for the cross-dehydrogenative coupling between 1,1-diphenylethylene and THF on the mixed oxide catalyst.

Notably, adding CeO_2 to the Cu-mediated reaction led to conflicting results, depending on the oxidation state of the present Cu species. Indeed, in the Cu(II)-mediated reactions, i.e., $\text{Cu}(\text{OAc})_2$, CuO , and the CuSi composite, poor yields of 21, 20, and 33%, respectively, were recorded; and due to the additional presence of CeO_2 , the production of 2-(2,2-diphenylvinyl)-tetrahydrofuran was significantly promoted to 43, 25, and 64%, respectively (Table 3, entries 5–10). Such yield enhancements suggested that Ce(IV) and Cu(II) species present in the same reaction have supporting impacts on the catalytic activity of each other, thus improving the transformation rate. However, the proposal should not be applied to the Cu(I) catalyst. A yield of 74% was obtained in the CuI-mediated reaction

and the combination of this catalytic system with CeO_2 resulted in a yield decrease to 64% (Entries 12 and 13).

The importance of the gel combustion method in the preparation of the catalyst was highlighted by the comparison of our composites with samples prepared by a mechanical mixture of the phases (Figure 12). CuO in the CuSi catalyst provided a much higher yield than the same amount of pure CuO , indicating much better accessibility of the catalytic sites. Importantly, the mixing of CeO_2 to CuO in nearly equal molar proportions caused limited increase of reaction yield to 25%, completely justified by the reactivity of the individual CuO and CeO_2 phases (respectively 20 and 30% yields). This allowed concluding that the large increase of reaction yield by the introduction of cerium in the composites was due to a better contact with CuO allowed by the gel-combustion method. Sun and co-workers suggested that CeO_2 with superior oxygen storage capacity could not only improve the dispersion of CuO species but could also interact with CuO , thus changing their physicochemical properties and enhancing the redox activity of the composite catalyst. Due to such strengthened synergistic effects in the CuO-CeO_2 composite, higher catalytic activities could be obtained in several different conversions compared to individual metal oxides [60,66,89,90].

2.2.3. Leaching Test and Recycling of the Heterogeneous Catalyst

As the liquid-phase synthesis of 2-(2,2-diphenylvinyl)-tetrahydrofuran from 1,1-diphenylethylene and THF via the cross-dehydrogenative coupling was catalyzed by a solid composite, it is crucial to investigate whether the catalysis proceeded under heterogeneous or homogeneous conditions. Indeed, in some cases, unstable species in a solid catalyst might migrate into the reaction medium, and such leached species might be active for the conversion. In order to clarify if leached species contributed to the total activity of the catalyst, a control experiment was performed. In detail, the reaction was conducted under standard conditions for 5 h. After the solids were then removed from the reaction mixture by centrifugation, the obtained liquid phase was analyzed by GC and transferred to a new 8-mL pressurized vial. The reaction mixture was added with an additional amount of KI and heated at 120 °C for another 20 h. The formation of the major product during this course was monitored by GC. It was observed that no more 2-(2,2-diphenylvinyl)tetrahydro-furan was detected after the removal of the $\text{Cu}_1\text{Ce}_{0.7}\text{Si}$ catalyst, indicating that the catalysis was truly heterogeneous and the leached species, if any, were inactive (Figure 14).

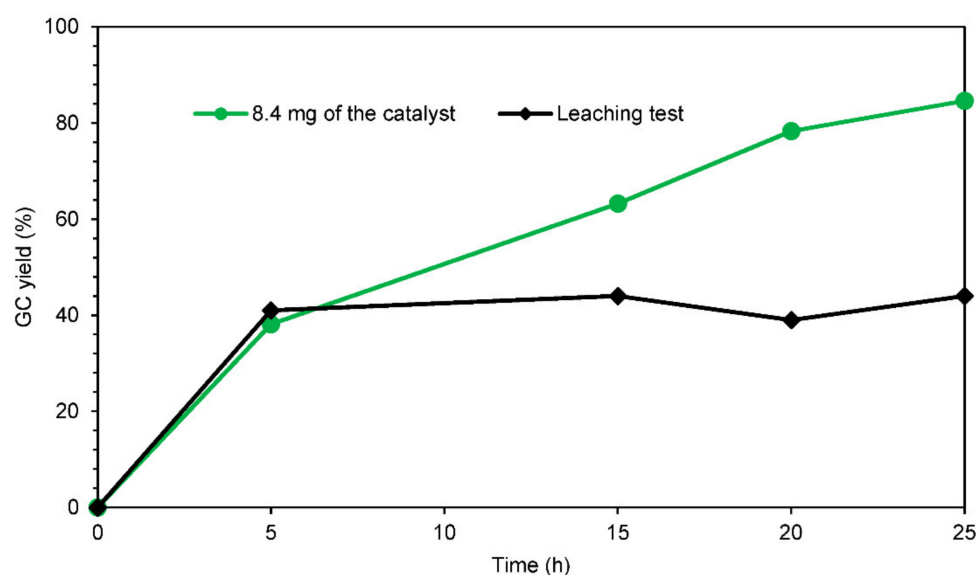


Figure 14. Leaching test for the $\text{Cu}_1\text{Ce}_{0.7}\text{Si}$ catalyst.

The development of heterogeneous catalytic systems for organic transformation could simplify product purification, minimize toxic wastes, and reduce synthetic expense. To highlight these advantages of using the composite catalyst rather than the unrecyclable metal salts-based catalysts previously reported for the dehydrogenative alkenylation, the reusability of the catalyst was explored. After the reaction course, the $\text{Cu}_1\text{Ce}_{0.7}\text{Si}$ catalyst was washed with ethyl acetate, acetone, and water and dried at 105 °C for 12 h before the next catalytic experiment. Just a minor decrease in the major product yield was observed in the fifth run, proving the high-efficiency recyclability of the composite for this transformation (Figure 15). The PXRD analysis for the catalyst after the fifth use showed that the crystalline structure of the oxides in the used composite was maintained compared to the fresh sample (Figure S3). Furthermore, via isothermal N_2 adsorption measurements, no significant change in the composite porosity was found with a surface area of $374 \text{ m}^2 \text{ g}^{-1}$. The elemental analysis indicated a constant Cu:Ce chemical composition for the used catalyst. With these results, it could be concluded that the $\text{CuO-CeO}_2\text{-SiO}_2$ composite was indeed stable under liquid-phase oxidative conditions.

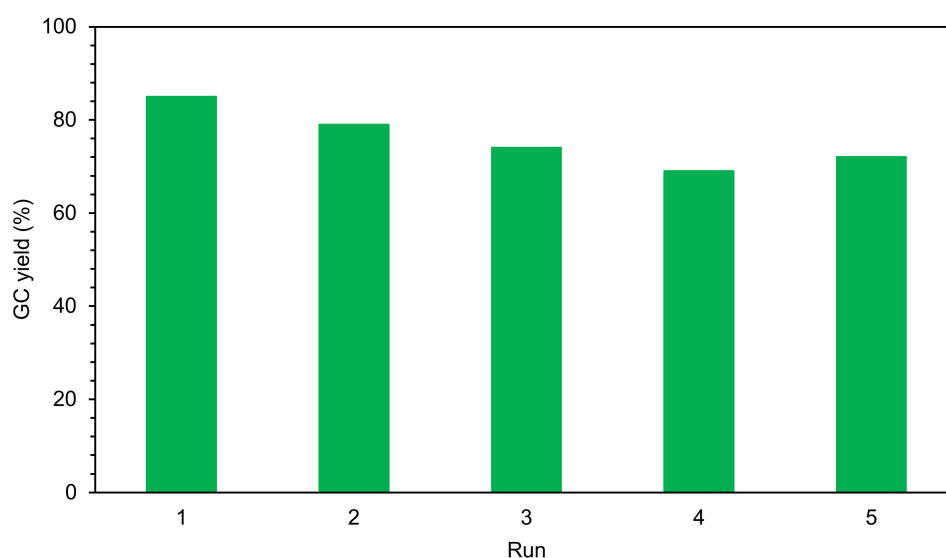


Figure 15. Recyclability test for the $\text{Cu}_1\text{Ce}_{0.7}\text{Si}$ catalyst.

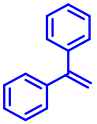

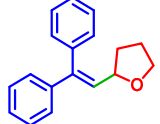
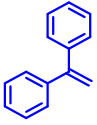
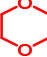
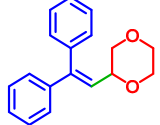
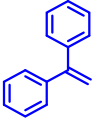
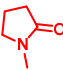
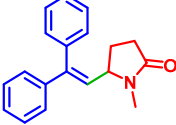
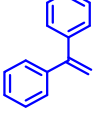
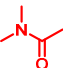
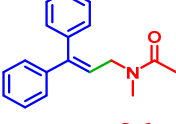
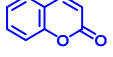
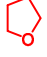
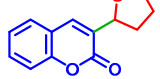
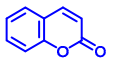
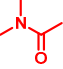
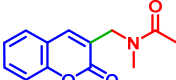
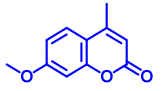
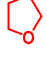
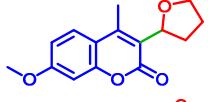
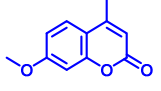
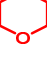
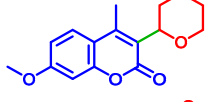
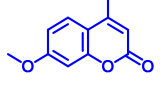
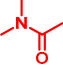
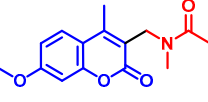
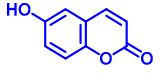

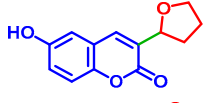
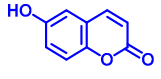

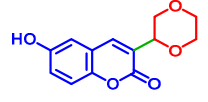
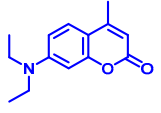
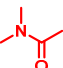
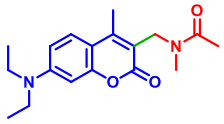
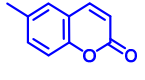
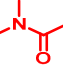
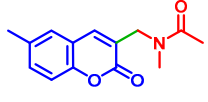
2.2.4. Dehydrogenative Coupling of Different Substrates

The study scope was subsequently expanded to the cross-dehydrogenative coupling reaction between different reactants using the composite catalyst (Table 4). The reaction was conducted at 120 °C for 25 h using 4.8 mol% of $\text{Cu}_1\text{Ce}_{0.7}\text{Si}$ with 4 equiv. of DTBP and 20 mol% of KI. The coupling products were then isolated by column chromatography.

First, the reactants containing $\text{C}(\text{sp}^3)\text{-H}$ adjacent to heteroatoms were tested. The selective alkenylation of THF by 1,1-diphenylethylene produced 2-(2,2-diphenylvinyl)-tetrahydrofuran in an isolated yield of 75% (Entry 1). When dioxane was used for the coupling reaction, 2-(2,2-diphenylvinyl)-1,4-dioxane was obtained with a yield of 70% (Entry 2). Interestingly, the reaction of *N*-methyl-2-pyrrolidone with 1,1-diphenylethylene showed high selectivity to the cyclic $\text{C}(\text{sp}^3)\text{-H}$ bond, giving 5-(2,2-diphenylvinyl)-1-methylpyrrolidin-2-one (65%, Entry 3) while a much lower yield of 30% was obtained for the case of *N,N*-dimethylacetamide. Coumarin-based compounds exhibit a wide range of biological activities and applications; therefore, in order to expand the substrate scope, the reactivity of the coumarins in this catalytic cross-dehydrogenative route was investigated [9,91,92]. Under the identical conditions, it was found that the C_3 position of coumarin could be directly functionalized with tetrahydrofuran and dimethylacetamide with yields of 28 and 58%, respectively. Furthermore, several substituted coumarins were selectively coupled with the

C(sp³)-H bond-containing compounds, affording the corresponding products in yields of 30–57% (Entries 7–13).

Table 4. Dehydrogenative alkenylation of C(sp³)-H adjacent to heteroatom catalyzed by the Cu₁Ce_{0.7}Si composite.

Entry	Reactant 1	Reactant 2	Product	Yield ^{[a], [b]} (%)
1				75
2				70
3				65
4				30
5				28
6				58
7				57
8				32
9				41
10				38
11				37
12				40
13				30

^[a] Reaction conditions: reactant 1 (0.3 mmol); reactant 2 (1 mL); DTBP (4 equiv.); KI (20 mol%); Cu₁Ce_{0.7}Si catalyst (8.4 mg); 120 °C; under air for 25 h. ^[b] Isolated yield.

3. Materials and Methods

3.1. Synthesis of Composites

The CuO-CeO₂-SiO₂ composites were synthesized via gel combustion. In a typical procedure, 1.519 g (6.3 mmol) of Cu(NO₃)₂·3H₂O and 1.892 g (4.4 mmol) of Ce(NO₃)₃·6H₂O were dissolved in 40 mL of ethanol under vigorous stirring at 25 °C in a ceramic crucible. Total of 17.338 g (83.2 mmol) of tetraethyl orthosilicate (TEOS) was subsequently added to the solution. The resulting mixture was stirred for another 30 min before slowly evaporated at 50 °C until a gel was obtained. For the combustion reaction, the crucible was then heated in convective air flow with a temperature ramp rate of 5 °C min⁻¹ and kept at 500 °C for 6 h. Eventually, this process yielded a grey porous solid denoted as, for instance, Cu₁Ce_{0.7}Si, in which 0.7 is the Ce/Cu molar ratio. Other samples with varied molar ratios of Cu:Ce were prepared according to the composition given in Table 1.

For comparison purposes, various catalysts purchased from Sigma-Aldrich (Saint-Louis, MO, USA) were also used, including CuI (98%), Cu(II) acetate (98%), CuO (99%), and CeO₂ (99%).

3.2. Characterization of As-Synthesized Composites

The textural properties of the materials were determined by nitrogen adsorption isotherm measurements at 77.4 K using a Micromeritics Tristar instrument. Before each analysis, samples were degassed at 150 °C under 10 Pa dynamic vacuum for 12 h. The specific surface area was determined using Brunauer–Emmett–Teller (BET) method by linearization across Point B [93]. The total pore volume was calculated at $P/P_0 = 0.99$ while the micropore volume was determined using the αS method.

Powder X-ray diffraction (PXRD) patterns were obtained on a D8 Advance Diffractometer (Bruker AXS, Karlsruhe, Germany) using a Ni-filtered CuK α radiation. Each measurement was performed in a 2θ range of 10–80° with an angular step size of 0.0105° and a scanning rate of 0.63° per min. The Scherrer method was used to calculate the average crystallite size of CuO and CeO₂.

Scanning electron microscopy (SEM) images were recorded on a TM 4000 Hitachi microscope equipped with an energy-dispersive X-ray spectroscopy (EDX) detector from Bruker. EDX mappings of some selected samples were performed to investigate the elemental distribution. Temperature-programmed reduction in H₂ (H₂-TPR) measurements were performed using a chemisorption analyzer AutoChem II 2920 (Micromeritics Instruments Corporation, Norcross, GA, USA) equipped with a thermal conductivity detector (TCD). Prior to each measurement, 50 mg of catalyst was loaded in a U-shape quartz reactor and pretreated at 150 °C (10 °C min⁻¹) for 30 min in 30 mL min⁻¹ of He flow, followed by cooling to 40 °C. Subsequently, a flow of 5 vol.% H₂/Ar (30 mL min⁻¹) was flown through the pretreated material. When the baseline was stable, the temperature was ramped up from 40 to 900 °C with a heating rate of 10 °C min⁻¹. The outlet gas duct was cooled by an ice bath before going to the TCD detector. The amount of H₂ consumption on each sample was calculated based on a comparison with the H₂ consumption from the reduction of standard CuO.

3.3. Catalytic Tests

In a typical experiment for the synthesis of 2-(2,2-diphenylvinyl)-tetrahydrofuran via cross-dehydrogenative coupling, 1,1-diphenylethylene (54.0 mg, 0.3 mmol), tetrahydrofuran (1 mL), potassium iodide (10.0 mg, 20 mol%), Cu₁Ce_{0.7}Si (5.6 mg, 3.2 mol%), and di-*tert*-butyl peroxide (DTBP, 0.22 mL, 1.2 mmol) were sequentially added to an 8-mL pressurized vial. The mole percent of reagents and catalyst (e.g., 3.2 mol% of Cu₁Ce_{0.7}Si) was based on the molar ratio of the metal sites (i.e., Cu and Ce) to 1,1-diphenylethylene. The reaction was then performed at 120 °C for 20 h under vigorous stirring. The reaction mixture was cooled to room temperature and then added with a pre-determined amount of diphenyl ether as an internal standard. An aliquot of the resulting mixture was withdrawn and quenched with brine (2.0 mL). The organic phase was extracted into ethyl

acetate (2.0 mL), dried over anhydrous Na_2SO_4 , filtered through a thin silica gel layer, and analyzed by gas chromatography to determine the yield of the reaction. The yield of 2-(2,2-diphenylvinyl)-tetrahydrofuran was determined using diphenyl ether as an internal standard.

Gas chromatographic (GC) analyses were performed on a GC 2010-Plus (Shimadzu, Kyoto, Japan) equipped with a flame ionization detector (FID) and an SPB-5 column (length = 30 m, inner diameter = 0.25 mm, and film thickness = 0.25 μm). The oven was first held at 100 $^\circ\text{C}$ for 1 min then heated from 100 $^\circ\text{C}$ to 280 $^\circ\text{C}$ with a ramp rate of 40 $^\circ\text{C min}^{-1}$ and held at 280 $^\circ\text{C}$ for another 4.5 min. The inlet and detector temperatures were constantly kept at 280 $^\circ\text{C}$.

To investigate catalyst recyclability, the catalyst was collected after the reaction by centrifugation, washed with excess amounts of acetone and water, dried at 105 $^\circ\text{C}$ for 12 h. The used catalyst was then tested for the next cycle under identical conditions.

3.4. Isolation and Identification of the Products

After the reaction, the resulting mixture was cooled to room temperature and then diluted with ethyl acetate (30 mL). The organic phase was washed with brine (3×10 mL). The organic layer was subsequently dried over anhydrous Na_2SO_4 , filtered through a thin silica gel layer, and concentrated under a reduced pressure. The product was isolated by column chromatography, using silica gel as a stationary phase and an ethyl acetate/hexane mixture (1/20 vol.) as an eluent, affording 2-(2,2-diphenylvinyl)-tetrahydrofuran as a clear liquid. The product structure was further confirmed by GC-MS, $^1\text{H-NMR}$, and $^{13}\text{C-NMR}$.

Mass spectra were collected on a GC-MS-QP2010 Ultra (Shimadzu, Kyoto, Japan) with a ZB-5MS column (length = 30 m, inner diameter = 0.25 mm, and film thickness = 0.25 μm). The oven was first held at 50 $^\circ\text{C}$ for 2 min, then heated from 50 to 280 $^\circ\text{C}$ with a ramp rate of 10 $^\circ\text{C min}^{-1}$ and held at 280 $^\circ\text{C}$ for another 10 min. Inlet temperature was constantly set at 280 $^\circ\text{C}$.

Nuclear magnetic resonance (NMR) spectra ($^1\text{H-NMR}$ and $^{13}\text{C-NMR}$) were recorded on a Bruker AV 500 spectrometer using residual solvent peaks as references.

4. Conclusions

In this work, a series of CuO-CeO-SiO_2 composites were facilely prepared using readily available precursors via the gel combustion method and then used as solid catalysts for the cross-dehydrogenative coupling reaction between $\text{C(sp}^2\text{)-H}$ and $\text{C(sp}^3\text{)-H}$ bonds. Due to strengthened synergistic effects and porous structure, the mixed oxide showed considerably higher activity for the transformation as compared to a mixture of single oxides. The catalyst could be reused many times and still afforded the major product in good yields. The structural characterizations indicated that the composite was indeed stable under liquid-phase oxidative conditions. The results of this study do not only indicate an efficient and simple approach to synthesize the highly porous CuO-CeO-SiO_2 composite but also expand the application area of this composite class to heterogeneous catalysis for liquid-phase organic conversions usually carried out by homogeneous catalysis.

Supplementary Materials: The following are available online at <https://www.mdpi.com/article/10.3390/catal11101252/s1>. Table S1: H_2 consumptions based on H_2 -TPR analysis. Figure S1: SEM/EDX elemental mapping images. Figure S2: pore size distribution results. Figure S3: PXRD pattern and N_2 -physisorption isotherm of the used catalyst. Figure S4: N_2 -physisorption isotherms of the fresh and used $\text{Cu}_1\text{Ce}_{0.7}\text{Si}$ catalysts. Figures S5–S30: $^1\text{H-}$ and $^{13}\text{C-NMR}$ spectra of the isolated coupling products.

Author Contributions: Conceptualization, H.V.L., P.H.H. and F.D.R.; formal analysis, K.D.N. and P.H.H.; investigation, V.B.N., H.H.P. and P.H.H.; methodology, H.V.L. and F.D.R.; supervision K.D.N. and P.T.; validation, V.B.N. and H.H.P.; writing—original draft, H.V.L.; writing—review and editing, P.H.H. and F.D.R. All authors have read and agreed to the published version of the manuscript.

Funding: This work is funded by The Vietnam National University—Ho Chi Minh City (VNU-HCM) via project No. NCM2019-20-01 (for Nam T. S. Phan).

Data Availability Statement: Data is contained within the article or Supplementary Materials.

Acknowledgments: We acknowledge Thu T. A. Le for experimental supports, Thuyet L. D. Pham for column chromatography experiences, and Tung T. Nguyen and Huy X. Le for valuable discussions on NMR analysis. P.H.H. is grateful to the European FEDER Readynov Solarvi for financial support. We would like to thank Ho Chi Minh City University of Technology (HCMUT), VNU-HCM for the support of time and facilities for this study.

Conflicts of Interest: The authors declare no conflict of interest.

References

1. Yeung, C.S.; Dong, V.M. Catalytic dehydrogenative cross-coupling: Forming carbon-carbon bonds by oxidizing two carbon-hydrogen bonds. *Chem. Rev.* **2011**, *111*, 1215–1292. [\[CrossRef\]](#)
2. Bras, J.L.; Muzart, J. Pd-Catalyzed Intermolecular Dehydrogenative Heck Reactions of Five-Membered Heteroarenes. *Catalysts* **2020**, *10*, 571. [\[CrossRef\]](#)
3. Bosque, I.; Chinchilla, R.; Gonzalez-Gomez, J.C.; Guijarro, D.; Alonso, F. Cross-dehydrogenative coupling involving benzylic and allylic C–H bonds. *Org. Chem. Front.* **2020**, *7*, 1717–1742. [\[CrossRef\]](#)
4. Huang, C.Y.; Kang, H.; Li, J.; Li, C.J. En Route to Intermolecular Cross-Dehydrogenative Coupling Reactions. *J. Org. Chem.* **2019**, *84*, 12705–12721. [\[CrossRef\]](#)
5. Niu, B.; Zhao, W.; Ding, Y.; Bian, Z.; Pittman, C.U.; Zhou, A.; Ge, H. Regioselective Cross-Couplings of Coumarins and Flavones with Ethers via C(sp³)–H Functionalization. *J. Org. Chem.* **2015**, *80*, 7251–7257. [\[CrossRef\]](#)
6. Zhang, M.; Yang, L.; Yang, H.; An, G.; Li, G. Visible Light Mediated C(sp³)–H Alkenylation of Cyclic Ethers Enabled by Aryl Ketone. *ChemCatChem* **2019**, *11*, 1606–1609. [\[CrossRef\]](#)
7. Gandhi, S. Catalytic enantioselective cross dehydrogenative coupling of sp(3) C–H of heterocycles. *Org. Biomol. Chem.* **2019**, *17*, 9683–9692. [\[CrossRef\]](#)
8. Guo, S.-R.; Kumar, P.S.; Yang, M. Recent Advances of Oxidative Radical Cross-Coupling Reactions: Direct α -C(sp³)–H Bond Functionalization of Ethers and Alcohols. *Adv. Synth. Catal.* **2017**, *359*, 2–25. [\[CrossRef\]](#)
9. Faisca Phillips, A.M.; Pombeiro, A.J.L. Recent Developments in Transition Metal-Catalyzed Cross-Dehydrogenative Coupling Reactions of Ethers and Thioethers. *ChemCatChem* **2018**, *10*, 3354–3383. [\[CrossRef\]](#)
10. He, C.; Whitehurst, W.G.; Gaunt, M.J. Palladium-Catalyzed C(sp³)–H Bond Functionalization of Aliphatic Amines. *Chem* **2019**, *5*, 1031–1058. [\[CrossRef\]](#)
11. Varun, B.V.; Dhineshkumar, J.; Bettadapur, K.R.; Siddaraju, Y.; Alagiri, K.; Prabhu, K.R. Recent advancements in dehydrogenative cross coupling reactions for CC bond formation. *Tetrahedron Lett.* **2017**, *58*, 803–824. [\[CrossRef\]](#)
12. Batra, A.; Singh, P.; Singh, K.N. Recent Advances in Functionalization of α -C(sp³)–H Centres in Inactivated Ethers through Cross Dehydrogenative Coupling. *Eur. J. Org. Chem.* **2017**, *2017*, 3739–3762. [\[CrossRef\]](#)
13. Liu, D.; Liu, C.; Li, H.; Lei, A. Copper-catalyzed oxidative C–H/C–H coupling between olefins and simple ethers. *Chem. Commun.* **2014**, *50*, 3623–3626. [\[CrossRef\]](#) [\[PubMed\]](#)
14. Dian, L.; Zhao, H.; Zhang-Negrerie, D.; Du, Y. Cobalt-Catalyzed Twofold Direct C(sp²)–C(sp³) Bond Coupling: Regioselective C-3 Alkylation of Coumarins with (Cyclo)alkyl Ethers. *Adv. Synth. Catal.* **2016**, *358*, 2422–2426. [\[CrossRef\]](#)
15. Trinh, K.H.; Tran, P.H.; Nguyen, T.T.; Doan, S.H.; Le, M.-V.; Nguyen, T.T.; Phan, N.T.S. Direct oxidative C(sp³)–H/C(sp²)–H coupling reaction using recyclable Sr-doped LaCoO₃ perovskite catalyst. *Appl. Organomet. Chem.* **2020**, *34*, e5515. [\[CrossRef\]](#)
16. Cam, T.S.; Vishnievskaya, T.A.; Popkov, V.I. Catalytic oxidation of CO over CuO/CeO₂ nanocomposites synthesized via solution combustion method: Effect of fuels. *Rev. Adv. Mater. Sci.* **2020**, *59*, 131–143. [\[CrossRef\]](#)
17. Liu, B.; Li, Y.; Cao, Y.; Wang, L.; Qing, S.; Wang, K.; Jia, D. Optimum Balance of Cu⁺ and Oxygen Vacancies of CuOx–CeO₂ Composites for CO Oxidation Based on Thermal Treatment. *Eur. J. Inorg. Chem.* **2019**, *2019*, 1714–1723. [\[CrossRef\]](#)
18. Chen, C.; Zhan, Y.; Zhou, J.; Li, D.; Zhang, Y.; Lin, X.; Jiang, L.; Zheng, Q. Cu/CeO₂ Catalyst for Water-Gas Shift Reaction: Effect of CeO₂ Pretreatment. *ChemPhysChem* **2018**, *19*, 1448–1455. [\[CrossRef\]](#)
19. Zhu, C.; Ding, T.; Gao, W.; Ma, K.; Tian, Y.; Li, X. CuO/CeO₂ catalysts synthesized from Ce–UiO-66 metal-organic framework for preferential CO oxidation. *Int. J. Hydrog. Energy* **2017**, *42*, 17457–17465. [\[CrossRef\]](#)
20. Montini, T.; Melchionna, M.; Monai, M.; Fornasiero, P. Fundamentals and Catalytic Applications of CeO₂-Based Materials. *Chem. Rev.* **2016**, *116*, 5987–6041. [\[CrossRef\]](#)
21. Hu, C.; Zhu, Q.; Jiang, Z.; Zhang, Y.; Wang, Y. Preparation and formation mechanism of mesoporous CuO–CeO₂ mixed oxides with excellent catalytic performance for removal of VOCs. *Microporous Mesoporous Mater.* **2008**, *113*, 427–434. [\[CrossRef\]](#)
22. Águila, G.; Gracia, F.; Araya, P. CuO and CeO₂ catalysts supported on Al₂O₃, ZrO₂, and SiO₂ in the oxidation of CO at low temperature. *Appl. Catal. A Gen.* **2008**, *343*, 16–24. [\[CrossRef\]](#)
23. Delimaris, D.; Ioannides, T. VOC oxidation over CuO–CeO₂ catalysts prepared by a combustion method. *Appl. Catal. B Environ.* **2009**, *89*, 295–302. [\[CrossRef\]](#)

24. Baidya, T.; Mazumder, T.; Koltunov, K.Y.; Likhar, P.R.; Clark, A.H.; Tiwari, K.; Sobolev, V.I.; Payra, S.; Murayama, T.; Lin, M.; et al. Low-Temperature Propylene Epoxidation Activity of CuO-CeO₂ Catalyst with CO + O₂: Role of Metal-Support Interaction on the Reducibility and Catalytic Property of CuOx Species. *J. Phys. Chem. C* **2020**, *124*, 14131–14146. [\[CrossRef\]](#)
25. Tiscornia, I.S.; Lacoste, A.M.; Gómez, L.E.; Boix, A.V. CuO-CeO₂/SiO₂ coating on ceramic monolith: Effect of the nature of the catalyst support on CO preferential oxidation in a H₂-rich stream. *Int. J. Hydrog. Energy* **2020**, *45*, 6636–6650. [\[CrossRef\]](#)
26. Akbar, M.; Tu, Z.; Jin, B.; Mushtaq, N.; He, Z.; Dong, W.; Wang, B.; Wang, X.; Xia, C. Demonstrating the dual functionalities of CeO₂-CuO composites in solid oxide fuel cells. *Int. J. Hydrog. Energy* **2020**, *46*, 9938–9947. [\[CrossRef\]](#)
27. The Luong, N.; Okumura, H.; Yamasue, E.; Ishihara, K.N. Structure and catalytic behaviour of CuO-CeO₂ prepared by high-energy ball milling. *R. Soc. Open Sci.* **2019**, *6*, 181861. [\[CrossRef\]](#)
28. Hossain, S.T.; Zell, E.T.; Balaz, S.; Wang, R. A γ to α type transition of CuO species over CeO₂-SiO₂ composites supported CuO catalysts. *Appl. Surf. Sci.* **2019**, *491*, 374–382. [\[CrossRef\]](#)
29. Shang, H.; Zhang, X.; Xu, J.; Han, Y. Effects of preparation methods on the activity of CuO/CeO₂ catalysts for CO oxidation. *Front. Chem. Sci. Eng.* **2017**, *11*, 603–612. [\[CrossRef\]](#)
30. Sedmak, G.; Hočevár, S.; Levec, J. Transient kinetic model of CO oxidation over a nanostructured Cu_{0.1}Ce_{0.9}O_{2-y} catalyst. *J. Catal.* **2004**, *222*, 87–99. [\[CrossRef\]](#)
31. Zedan, A.F.; Aljaber, A.S. Combustion Synthesis of Non-Precious CuO-CeO(2) Nanocrystalline Catalysts with Enhanced Catalytic Activity for Methane Oxidation. *Materials* **2019**, *12*, 878. [\[CrossRef\]](#)
32. Prasad, R.; Rattan, G. Preparation Methods and Applications of CuO-CeO₂ Catalysts: A Short Review. *Bull. Chem. React. Eng. Catal.* **2010**, *5*, 7–30. [\[CrossRef\]](#)
33. Piumetti, M.; Bensaid, S.; Andana, T.; Russo, N.; Pirone, R.; Fino, D. Cerium-copper oxides prepared by solution combustion synthesis for total oxidation reactions: From powder catalysts to structured reactors. *Appl. Catal. B Environ.* **2017**, *205*, 455–468. [\[CrossRef\]](#)
34. Liu, G.; Chen, K.; Li, J. Combustion synthesis: An effective tool for preparing inorganic materials. *Scr. Mater.* **2018**, *157*, 167–173. [\[CrossRef\]](#)
35. Thoda, O.; Xanthopoulou, G.; Vekinis, G.; Chroneos, A. Review of Recent Studies on Solution Combustion Synthesis of Nanostructured Catalysts. *Adv. Eng. Mater.* **2018**, *20*, 1800047. [\[CrossRef\]](#)
36. Novitskaya, E.; Kelly, J.P.; Bhaduri, S.; Graeve, O.A. A review of solution combustion synthesis: An analysis of parameters controlling powder characteristics. *Int. Mater. Rev.* **2021**, *66*, 188–214. [\[CrossRef\]](#)
37. Carlos, E.; Martins, R.; Fortunato, E.; Branquinho, R. Solution Combustion Synthesis: Towards a Sustainable Approach for Metal Oxides. *Chemistry* **2020**, *26*, 9099–9125. [\[CrossRef\]](#)
38. Xanthopoulou, G.; Thoda, O.; Roslyakov, S.; Steinman, A.; Kovalev, D.; Levashov, E.; Vekinis, G.; Sytschev, A.; Chroneos, A. Solution combustion synthesis of nano-catalysts with a hierarchical structure. *J. Catal.* **2018**, *364*, 112–124. [\[CrossRef\]](#)
39. Deganello, F.; Tyagi, A.K. Solution combustion synthesis, energy and environment: Best parameters for better materials. *Prog. Cryst. Growth Charact. Mater.* **2018**, *64*, 23–61. [\[CrossRef\]](#)
40. Varma, A.; Mukasyan, A.S.; Rogachev, A.S.; Manukyan, K.V. Solution Combustion Synthesis of Nanoscale Materials. *Chem. Rev.* **2016**, *116*, 14493–14586. [\[CrossRef\]](#)
41. Li, F.T.; Ran, J.; Jaroniec, M.; Qiao, S.Z. Solution combustion synthesis of metal oxide nanomaterials for energy storage and conversion. *Nanoscale* **2015**, *7*, 17590–17610. [\[CrossRef\]](#)
42. Bera, P.; Aruna, S.T.; Patil, K.C.; Hegde, M.S. Studies on Cu/CeO₂: A New NO Reduction Catalyst. *J. Catal.* **1999**, *186*, 36–44. [\[CrossRef\]](#)
43. Purohit, R.D.; Sharma, B.P.; Pillai, K.T.; Tyagi, A.K. Ultrafine ceria powders via glycine-nitrate combustion. *Mater. Res. Bull.* **2001**, *36*, 2711–2721. [\[CrossRef\]](#)
44. Hu, T.; Yang, J.; Zhao, J.; Wang, D.; Song, H.; Chou, L. Preparation of a Cu-Ce-O Catalyst by Urea Combustion for Removing CO from Hydrogen. *Chin. J. Catal.* **2007**, *28*, 844–846. [\[CrossRef\]](#)
45. Marbán, G.; Fuertes, A.B. Highly active and selective CuOx/CeO₂ catalyst prepared by a single-step citrate method for preferential oxidation of carbon monoxide. *Appl. Catal. B Environ.* **2005**, *57*, 43–53. [\[CrossRef\]](#)
46. Avgouropoulos, G.; Ioannides, T. Selective CO oxidation over CuO-CeO₂ catalysts prepared via the urea-nitrate combustion method. *Appl. Catal. A Gen.* **2003**, *244*, 155–167. [\[CrossRef\]](#)
47. Luo, J.; Chu, W.; Xu, H.; Jiang, C.; Zhang, T. Low-temperature CO oxidation over CuO-CeO₂/SiO₂ catalysts: Effect of CeO₂ content and carrier porosity. *J. Nat. Gas Chem.* **2010**, *19*, 355–361. [\[CrossRef\]](#)
48. DeHoff, R.T.; Rummel, R.A.; LaBuff, H.P.; Rhines, F.N. The Relationship Between Surface Area and Density in the Second-Stage Sintering of Metals. In *Modern Developments in Powder Metallurgy*; Hausner, H.H., Ed.; Springer: Boston, MA, USA, 1966.
49. Shi, L.; Yang, R.-Q.; Tao, K.; Yoneyama, Y.; Tan, Y.-S.; Tsubaki, N. Surface impregnation combustion method to prepare nanostructured metallic catalysts without further reduction: As-burnt Cu-ZnO/SiO₂ catalyst for low-temperature methanol synthesis. *Catal. Today* **2012**, *185*, 54–60. [\[CrossRef\]](#)
50. Reddy, B.M.; Reddy, G.K.; Ganesh, I.; Ferreira, J.M.F. Single step synthesis of nanosized CeO₂-MxOy mixed oxides (MxOy = SiO₂, TiO₂, ZrO₂, and Al₂O₃) by microwave induced solution combustion synthesis: Characterization and CO oxidation. *J. Mater. Sci.* **2009**, *44*, 2743–2751. [\[CrossRef\]](#)

51. Voskanyan, A.A.; Chan, K.-Y.; Li, C.-Y.V. Colloidal Solution Combustion Synthesis: Toward Mass Production of a Crystalline Uniform Mesoporous CeO₂ Catalyst with Tunable Porosity. *Chem. Mater.* **2016**, *28*, 2768–2775. [\[CrossRef\]](#)
52. Papavasiliou, A.; Tsiourvas, D.; Deze, E.G.; Papageorgiou, S.K.; Katsaros, F.K.; Poulakis, E.; Philippopoulos, C.J.; Boukos, N.; Xin, Q.; Cool, P. Hyperbranched polyethyleneimine towards the development of homogeneous and highly porous CuO-CeO₂-SiO₂ catalytic materials. *Chem. Eng. J.* **2016**, *300*, 343–357. [\[CrossRef\]](#)
53. Cannas, C.; Musinu, A.; Peddis, D.; Piccaluga, G. Synthesis and Characterization of CoFe₂O₄ Nanoparticles Dispersed in a Silica Matrix by a Sol–Gel Autocombustion Method. *Chem. Mater.* **2006**, *18*, 3835–3842. [\[CrossRef\]](#)
54. Amaniampong, P.N.; Trinh, Q.T.; Li, K.; Mushrif, S.H.; Hao, Y.; Yang, Y. Porous structured CuO-CeO₂ nanospheres for the direct oxidation of cellobiose and glucose to gluconic acid. *Catal. Today* **2018**, *306*, 172–182. [\[CrossRef\]](#)
55. Liu, W.; Flytzanistephanopoulos, M. Total Oxidation of Carbon Monoxide and Methane over Transition Metal Fluorite Oxide Composite Catalysts: I. Catalyst Composition and Activity. *J. Catal.* **1995**, *153*, 304–316. [\[CrossRef\]](#)
56. Wang, Z.-Q.; Xu, Z.-N.; Peng, S.-Y.; Zhang, M.-J.; Lu, G.; Chen, Q.-S.; Chen, Y.; Guo, G.-C. High-Performance and Long-Lived Cu/SiO₂ Nanocatalyst for CO₂ Hydrogenation. *ACS Catal.* **2015**, *5*, 4255–4259. [\[CrossRef\]](#)
57. Le, H.V.; Parishan, S.; Sagaltchik, A.; Ahi, H.; Trunschke, A.; Schomäcker, R.; Thomas, A. Stepwise Methane-to-Methanol Conversion on CuO/SBA-15. *Chem. A Eur. J.* **2018**, *24*, 12592–12599. [\[CrossRef\]](#)
58. Ho, P.H.; Ambrosetti, M.; Groppi, G.; Tronconi, E.; Fornasari, G.; Vaccari, A.; Benito, P. Electrodeposition of CeO₂ and Pd-CeO₂ on small pore size metallic foams: Selection of deposition parameters. *Catal. Today* **2019**, *334*, 37–47. [\[CrossRef\]](#)
59. Astudillo, J.; Águila, G.; Diaz, F.; Guerrero, S.; Araya, P. Study of CuO-CeO₂ catalysts supported on SiO₂ on the low-temperature oxidation of CO. *Appl. Catal. A Gen.* **2010**, *381*, 169–176. [\[CrossRef\]](#)
60. Sun, S.; Mao, D.; Yu, J.; Yang, Z.; Lu, G.; Ma, Z. Low-temperature CO oxidation on CuO/CeO₂ catalysts: The significant effect of copper precursor and calcination temperature. *Catal. Sci. Technol.* **2015**, *5*, 3166–3181. [\[CrossRef\]](#)
61. Qi, L.; Yu, Q.; Dai, Y.; Tang, C.; Liu, L.; Zhang, H.; Gao, F.; Dong, L.; Chen, Y. Influence of cerium precursors on the structure and reducibility of mesoporous CuO-CeO₂ catalysts for CO oxidation. *Appl. Catal. B Environ.* **2012**, *119–120*, 308–320. [\[CrossRef\]](#)
62. Ratnasamy, P.; Srinivas, D.; Satyanarayana, C.V.V.; Manikandan, P.; Senthil Kumaran, R.S.; Sachin, M.; Shetti, V.N. Influence of the support on the preferential oxidation of CO in hydrogen-rich steam reformates over the CuO-CeO₂-ZrO₂ system. *J. Catal.* **2004**, *221*, 455–465. [\[CrossRef\]](#)
63. Le, H.V.; Parishan, S.; Sagaltchik, A.; Göbel, C.; Schlesiger, C.; Malzer, W.; Trunschke, A.; Schomäcker, R.; Thomas, A. Solid-State Ion-Exchanged Cu/Mordenite Catalysts for the Direct Conversion of Methane to Methanol. *ACS Catal.* **2017**, *7*, 1403–1412. [\[CrossRef\]](#)
64. Cargnello, M.; Doan-Nguyen, V.V.T.; Gordon, T.R.; Diaz, R.E.; Stach, E.A.; Gorte, R.J.; Fornasiero, P.; Murray, C.B. Control of Metal Nanocrystal Size Reveals Metal-Support Interface Role for Ceria Catalysts. *Science* **2013**, *341*, 771–773. [\[CrossRef\]](#)
65. Albonetti, S.; Lolli, A.; Morandi, V.; Migliori, A.; Lucarelli, C.; Cavani, F. Conversion of 5-hydroxymethylfurfural to 2,5-furandicarboxylic acid over Au-based catalysts: Optimization of active phase and metal-support interaction. *Appl. Catal. B-Environ.* **2015**, *163*, 520–530. [\[CrossRef\]](#)
66. Gamarra, D.; Belver, C.; Fernández-García, M.; Martínez-Arias, A. Selective CO Oxidation in Excess H₂ over Copper–Ceria Catalysts: Identification of Active Entities/Species. *J. Am. Chem. Soc.* **2007**, *129*, 12064–12065. [\[CrossRef\]](#)
67. Gamarra, D.; Munuera, G.; Hungria, A.B.; Fernández-García, M.; Conesa, J.C.; Midgley, P.A.; Wang, X.Q.; Hanson, J.C.; Rodríguez, J.A.; Martínez-Arias, A. Structure–Activity Relationship in Nanostructured Copper–Ceria-Based Preferential CO Oxidation Catalysts. *J. Phys. Chem. C* **2007**, *111*, 11026–11038. [\[CrossRef\]](#)
68. Aguila, G.; Guerrero, S.; Araya, P. Effect of the preparation method and calcination temperature on the oxidation activity of CO at low temperature on CuO-CeO₂/SiO₂ catalysts. *Appl. Catal. A Gen.* **2013**, *462–463*, 56–63. [\[CrossRef\]](#)
69. Song, Y.-Y.; Du, L.-Y.; Wang, W.-W.; Jia, C.-J. CeO₂@SiO₂ Core-Shell Nanostructure-Supported CuO as High-Temperature-Tolerant Catalysts for CO Oxidation. *Langmuir* **2019**, *35*, 8658–8666. [\[CrossRef\]](#) [\[PubMed\]](#)
70. Ho, P.H.; Jabłońska, M.; Beltrami, G.; Martucci, A.; Cacciaguerra, T.; Paulus, W.; Di Renzo, F.; Fornasari, G.; Vaccari, A.; Benito, P.; et al. Promotion effect of rare earth elements (Ce, Nd, Pr) on physicochemical properties of M-Al mixed oxides (M = Cu, Ni, Co) and their catalytic activity in N₂O decomposition. *J. Mater. Sci.* **2021**, *56*, 15012–15028. [\[CrossRef\]](#)
71. Giordano, F.; Trovarelli, A.; de Leitenburg, C.; Giona, M. A Model for the Temperature-Programmed Reduction of Low and High Surface Area Ceria. *J. Catal.* **2000**, *193*, 273–282. [\[CrossRef\]](#)
72. Zimmer, P.; Tschöpe, A.; Birringer, R. Temperature-Programmed Reaction Spectroscopy of Ceria- and Cu/Ceria-Supported Oxide Catalyst. *J. Catal.* **2002**, *205*, 339–345. [\[CrossRef\]](#)
73. Thommes, M.; Kaneko, K.; Neimark, A.V.; Olivier, J.P.; Rodriguez-Reinoso, F.; Rouquerol, J.; Sing, K.S.W. Physisorption of gases, with special reference to the evaluation of surface area and pore size distribution (IUPAC Technical Report). *Pure Appl. Chem.* **2015**, *87*, 1051–1069. [\[CrossRef\]](#)
74. Meixner, D.L.; Dyer, P.N. Influence of Sol-Gel Synthesis Parameters on the Microstructure of Particulate Silica Xerogels. *J. Sol-Gel Sci. Technol.* **1999**, *14*, 223–232. [\[CrossRef\]](#)
75. Newalkar, B.L.; Komarneni, S. Synthesis and Characterization of Microporous Silica Prepared with Sodium Silicate and Organosilane Compounds. *J. Sol-Gel Sci. Technol.* **2000**, *18*, 191–198. [\[CrossRef\]](#)

76. Aerts, C.A.; Verraedt, E.; Mellaerts, R.; Depla, A.; Augustijns, P.; Van Humbeeck, J.; Van den Mooter, G.; Martens, J.A. Tunability of Pore Diameter and Particle Size of Amorphous Microporous Silica for Diffusive Controlled Release of Drug Compounds. *J. Phys. Chem. C* **2007**, *111*, 13404–13409. [\[CrossRef\]](#)
77. Sebbar, N.; Bozzelli, J.W.; Bockhorn, H. Kinetic Study of Di-Tert-Butyl Peroxide: Thermal Decomposition and Product Reaction Pathways. *Int. J. Chem. Kinet.* **2015**, *47*, 133–161. [\[CrossRef\]](#)
78. RajanBabu, T.V.; Simpkins, N.S.; RajanBabu, T.V. 1,1-Di-tert-butyl Peroxide. In *Encyclopedia of Reagents for Organic Synthesis*; John Wiley & Sons: Hoboken, NJ, USA, 2005.
79. Chu, X.-Q.; Ge, D.; Shen, Z.-L.; Loh, T.-P. Recent Advances in Radical-Initiated C(sp³)-H Bond Oxidative Functionalization of Alkyl Nitriles. *ACS Catal.* **2017**, *8*, 258–271. [\[CrossRef\]](#)
80. Cao, H.; Liu, D.; Liu, C.; Hu, X.; Lei, A. Copper-catalyzed oxidative alkenylation of thioethers via Csp(3)-H functionalization. *Org. Biomol. Chem.* **2015**, *13*, 2264–2266. [\[CrossRef\]](#) [\[PubMed\]](#)
81. Wang, C.; Gong, M.; Huang, M.; Li, Y.; Kim, J.K.; Wu, Y. Copper-mediated alkylation of furan and thiophene derivatives with cyclic ethers. *Tetrahedron* **2016**, *72*, 7931–7936. [\[CrossRef\]](#)
82. Trinh, K.H.; Doan, S.H.; Huynh, T.V.; Tran, P.H.; Pham, D.N.; Le, M.V.; Nguyen, T.T.; Phan, N.T.S. Alternative pathways to alpha,beta-unsaturated ketones via direct oxidative coupling transformation using Sr-doped LaCoO₃ perovskite catalyst. *R. Soc. Open Sci.* **2019**, *6*, 191313. [\[CrossRef\]](#)
83. Wang, C.; Mi, X.; Li, Q.; Li, Y.; Huang, M.; Zhang, J.; Wu, Y.; Wu, Y. Copper-catalyzed cross-dehydrogenative-coupling (CDC) of coumarins with cyclic ethers and cycloalkane. *Tetrahedron* **2015**, *71*, 6689–6693. [\[CrossRef\]](#)
84. Nam, W.; Han, H.J.; Oh, S.-Y.; Lee, Y.J.; Choi, M.-H.; Han, S.-Y.; Kim, C.; Woo, S.K.; Shin, W. New Insights into the Mechanisms of O–O Bond Cleavage of Hydrogen Peroxide and tert-Alkyl Hydroperoxides by Iron(III) Porphyrin Complexes. *J. Am. Chem. Soc.* **2000**, *122*, 8677–8684. [\[CrossRef\]](#)
85. Gevorgyan, V.; Priede, E.; Liepiņš, E.; Gavars, M.; Lukevics, E. Radical addition of tetrahydrofuran and tetrahydro-2-furanone to alkenylsilanes in the presence of di(t-butyl)peroxide. *J. Organomet. Chem.* **1990**, *393*, 333–338. [\[CrossRef\]](#)
86. Wu, X.; Wang, M.; Zhang, G.; Zhao, Y.; Wang, J.; Ge, H. Copper-catalyzed diastereoselective aerobic intramolecular dehydrogenative coupling of hydrazones via sp(3) C-H functionalization. *Chem. Sci.* **2015**, *6*, 5882–5890. [\[CrossRef\]](#) [\[PubMed\]](#)
87. Imrich, H.-G.; Conrad, J.; Beifuss, U. Copper-Catalyzed Double Intramolecular Ullmann Coupling for the Synthesis of Diastereomerically and Enantiomerically Pure 4b,9b-Dihydrobenzofuro[3,2-b]benzofurans. *Eur. J. Org. Chem.* **2015**, *2015*, 7718–7734. [\[CrossRef\]](#)
88. Maaliki, C.; Thiery, E.; Thibonnet, J. Emergence of Copper-Mediated Formation of C-C Bonds. *Eur. J. Org. Chem.* **2017**, *2017*, 209–228. [\[CrossRef\]](#)
89. Li, J.; Han, Y.; Zhu, Y.; Zhou, R. Purification of hydrogen from carbon monoxide for fuel cell application over modified mesoporous CuO-CeO₂ catalysts. *Appl. Catal. B Environ.* **2011**, *108–109*, 72–80. [\[CrossRef\]](#)
90. Melchionna, M.; Fornasiero, P. The role of ceria-based nanostructured materials in energy applications. *Mater. Today* **2014**, *17*, 349–357. [\[CrossRef\]](#)
91. Srikrishna, D.; Godugu, C.; Dubey, P.K. A Review on Pharmacological Properties of Coumarins. *Mini Rev. Med. Chem.* **2018**, *18*, 113–141. [\[CrossRef\]](#)
92. Pereira, T.M.; Franco, D.P.; Vitorio, F.; Kummerle, A.E. Coumarin Compounds in Medicinal Chemistry: Some Important Examples from the Last Years. *Curr. Top. Med. Chem.* **2018**, *18*, 124–148. [\[CrossRef\]](#)
93. Rouquerol, F.; Rouquerol, J.; Sing, K. CHAPTER 6—Assessment of Surface Area. In *Adsorption by Powders and Porous Solids*; Rouquerol, F., Rouquerol, J., Sing, K., Eds.; Academic Press: London, UK, 1999; pp. 165–189.